A novel Notch and WNT signaling mechanism contribute to paediatric DCM: a pathway to new therapeutics.

Obed O. Nyarko, MD[1, 2], Ethan Rausch, BS[2], Jared R.H. Goff, BS[3], Anis Karimpour-Fard, PhD[4], Caitlyn S. Conard, BS[2], Laura Hernandez-Lagunas, MS[2], McKenna P.A. Burns, PhD[2], Brisa Peña, PhD[2,5], Shelley D. Miyamoto, MD[6*], Brian L. Stauffer, MD[2*], Carmen C. Sucharov, PhD[2*#].

[1]Integrative Physiology Graduate Program, University of Colorado Anschutz Medical Campus, Aurora, CO 80045, USA.

[2]Department of Medicine, Division of Cardiology, University of Colorado Anschutz Medical Campus, Aurora, CO 80045, USA.

[3]University of Utah Department of Internal Medicine.

[4]Department of Medicine, Division of General Internal Medicine, University of Colorado School of Medicine, Aurora, CO, 80045.

[5]Bioengineering Department, University of Colorado Denver Anschutz Medical Campus, Aurora, Colorado, 80045.

[6]Department of Paediatrics, Division of Cardiology, University of Colorado Anschutz Medical Campus, Aurora, CO 80045, USA.

Short title: Novel mechanism of DCM via Notch and WNT.

*These authors contributed equally to the study conceptualization and experimental planning.

[#]**Corresponding author:**

Carmen C. Sucharov. 12700 E. 19th Ave., B-139 Aurora, Aurora, CO 80045, USA.

kika.sucharov@cuanschutz.edu

ABSTRACT

Background

Paediatric Idiopathic dilated cardiomyopathy (iDCM) is a life-threatening disease. The lack of disease-specific animal models limits our understanding of its mechanisms. We previously demonstrated that paediatric iDCM serum-circulating proteins promote pathologic remodeling *in vitro*, and that secreted frizzled related protein 1 (sFRP1) increases stiffness in cardiomyocytes. Here we investigated the mechanisms by which sFRP1 contributes to iDCM.

Methods

The effect of sFRP1 in combination with isoproterenol (ISO) (to recapitulate the increase in circulating catecholamine observed in paediatric iDCM) was evaluated in neonatal rat ventricular myocytes (*in vitro*), and in neonatal rats through intraperitoneal injections (*in vivo*). Function and molecular mechanisms were investigated through echocardiography and next-generation-sequencing. Protein levels and localization were determined by Western blot. Tissue stiffness was measured by Atomic Force Microscopy. *In vitro* and *in vivo* data were compared to explanted human heart tissue.

Results

We show that ISO+sFRP1 reactivates the fetal gene program *in vitro,* and promotes cardiac dysfunction, dilation and stiffness *in vivo*. Importantly, we show stiffness is also increased in paediatric iDCM hearts. We identified co-activation of Notch and WNT signaling in both ISO+sFRP1-treated rats and paediatric iDCM hearts. Mechanistically, *in vitro* inhibition of Notch or β-catenin prevented pathological remodeling, and Notch

inhibition improved cardiac function, myocardial stiffness and ventricular dilation in ISO+sFRP1-treated rats.

Conclusion

We identified alterations in Notch and WNT signaling in paediatric iDCM hearts and in our model. Notch inhibition abrogated pathologic changes *in vitro* and *in vivo*. These findings provide novel mechanistic insights and a potential therapeutic target for paediatric iDCM.

Keywords- Paediatric, Heart failure, dilated cardiomyopathy, stiffness, Notch, WNT,

Graphical abstract

Text element:

- **Key Question-** Age-specific disease mechanisms may explain the heterogenous response of paediatric iDCM patients to standard heart failure therapies that are effective in adults.
- **Key Finding-** This study identifies Notch and WNT as important pathways altered in paediatric DCM. Additionally, it establishes a unique young rat model of the disease that recapitulates important aspects of paediatric iDCM, including an increase in cardiac stiffness.
- **Take-home Message-** This study uncovers a potential therapeutic target of paediatric DCM via Notch inhibition.

Translational perspective

Idiopathic dilated cardiomyopathy (iDCM) in children continues to be poorly understood. This study investigates molecular pathways altered in paediatric iDCM and establishes a unique young rat model that recapitulates key features of the disease. These features include impaired systolic function with ventricular dilation, myocardial stiffness and distinct transcriptomic signatures. We identified Notch and WNT co-activation as key regulators of pathological remodeling and cardiac dysfunction and show that inhibition of Notch signaling can prevent pathological remodeling and cardiac dysfunction. These findings provide a preclinical model to investigate targeted interventions for paediatric iDCM.

INTRODUCTION

Idiopathic dilated cardiomyopathy (iDCM) is one of the main causes of cardiac-related mortality in children[1]. Unfortunately, to date, there is limited evidence to support the treatment of HF in children, and current therapies are largely based on extrapolation of guideline-directed medical therapy (GDMT) for adult patients without proven efficacy in children[2].

Existing animal models of HF in children tend to focus on specific genetic mutations. However, only about one-third of children with iDCM have any identified pathogenic genetic variant[3], making use of any single genetic model difficult to generalize to the paediatric iDCM population. The lack of a generalizable animal model has negatively impacted the ability to investigate mechanisms of disease and identify targeted therapeutic options, which likely contributes to the fact that paediatric HF outcomes lag behind those of adults[4].

In the pathological state, the heart responds by reverting to the fetal gene program (FGP)[5], which includes re-expression of natriuretic peptides (*NPPA*/*NPPB*) and reduced expression of the ratio α/β-Myosin Heavy Chain (MHC–*Myh6/Myh7*)[5,6]. We tested the effect of the paediatric iDCM secretome on gene expression and cellular stiffness in primary cardiomyocytes and showed that circulating proteins contribute to pathologic changes in cells[7]. We further showed that the protein secreted frizzled protein 1 (sFRP1) is increased in the serum and hearts of patients with iDCM and promoted cellular stiffness in primary cardiomyocytes[7]. sFRP1 is known to modulate the WNT

signaling pathway[8]. WNT ligands regulate cellular activities through the activation of β-catenin-dependent (canonical) and independent (non-canonical) pathways[8]. The WNT signaling pathway influences Notch signaling activity in various cellular and developmental contexts. In cardiogenesis, both WNT and Notch signaling pathways are crucial in determining cell fate and survival[9,10]. The activity of Notch signaling is usually reduced in the postnatal heart but increased in cases of damage or injury[11]. Activation of the Notch receptors and subsequent cleavage by ADAM metalloproteinases and γ-secretase leads to the release of the Notch intracellular domain (NICD) in the cytoplasm, which translocates to the nucleus and activates transcription of Notch target genes resulting in cell specific effects[9].

In this study we investigated the effect of sFRP1 *in vitro* and *in vivo* through the development of a novel animal model that consists of intraperitoneal injections of sFRP1 and isoproterenol (to recapitulate the increase in circulating catecholamine observed in paediatric iDCM patients)[12,13]. We show that this model reproduces aspects of paediatric iDCM, including decreased cardiac function associated with dilation, and activation of Notch and WNT signaling. We further show that ISO+sFRP1 promotes cardiac stiffness, and importantly, inhibiting Notch signaling prevents pathological remodeling and cardiac dysfunction.

METHODS (Extensively described in Supplementary material).

Human tissue collection was approved by the University of Colorado Anschutz Medical Campus COMIRB and complies with the Declaration of Helsinki.

Cell culture

NRVMs were prepared from 1 to 3-day old rats as described by our group[7] and were treated for 72 hours prior to harvesting.

RNA extraction and real-time quantitative PCR.

NRVMs were homogenized in Qiazol (QIAGEN), and RNA was extracted as described[7,14]. Gene expression was measured by real-time quantitative PCR (RT-qPCR) as previously described[7]

Protein extraction and nuclear/cytoplasmic fractionation

Total protein was extracted from cells using RIPA40 (Pierce RIPA Buffer, FisherScientific, PI89900). Nuclear and cytoplasmic fractions were purified using NE-PER (FisherScientific, 78835)[7,15–17]. Western blots were performed essentially as previously described[16,18].

Neonatal rat injections

All animal studies were in compliance with the *Guide for the Care and Use of Laboratory Animals* (National Academies Press, 2011) and approved by the IACUC of the University of Colorado Anschutz Medical Campus. Animal protocols are in accordance with PHS Animal Welfare Assurance (A3269-01). Pregnant Sprague Dawley female rats were purchased from Charles Rivers laboratories. Transthoracic echocardiograms (EchoPAC SW v201), isolation of myocardium and AFM assessment of cardiac stiffness were done as extensively described by our group[19,20].

Bulk RNA-sequencing

Total RNA was extracted from the LV tissue of rats (n=6/group). Samples with an RNA integrity number greater than 9 were considered to be suitable for RNA-Seq. RNA-sequencing reads were obtained using the Illumina HiSeq analysis pipeline.

Single nuclei RNA-Sequencing and nuclei isolation

Nuclei were isolated from LV tissue of rats (n=3/group) using the Chromium Nuclei Isolation Kit (10x Genomics, PN-1000494) as described in[22]**.** Reverse transcription, barcoding, complementary DNA amplification and purification for library preparation were performed by the Genomics Core at CU Anschutz using the 10X Genomics Chromium technology. Generated libraries were sequenced on the Illumina NovaSeq 6000 instrument. Data processing downstream was performed in the R package Seurat (v4)[23].

Statistical Analysis

Data are presented as mean±SEM. Comparisons between two groups were made using unpaired two-tailed *t*-test. For comparisons involving more than two groups, one-way ANOVA with Tukey's post hoc test was used as appropriate. Significance is defined as $p<0.05$.

RESULTS

Human Samples

Detailed demographics for all patients included in the study are depicted in Supplemental Table 1. Median age for DCM patients was 3.9 years (interquartile range-IQR=6.2), with an average ejection fraction (EF) of 17.33%, 58.3% were female, 8.3% were on beta-blockers, all were on angiotensin converting enzyme inhibitors and 75%

were on a phosphodiesterase 3-inhibitor. Non-failing control (NF) subjects had a median age of 6.9 years (IQR=9.5), 28.6% were female and 14.3% were on beta-blockers.

ISO+sFRP1 treatment promotes pathological remodeling *in vitro*

We first evaluated if treatment with ISO and/or sFRP1 promoted pathological remodeling i*n vitro*. Neonatal rat ventricular myocytes (NRVMs) were treated with ISO, sFRP1 or a combination of both factors for 72 hours. Activation of all genes of the fetal gene program (FGP), as measured by upregulation of *NPPA, NPPB*, and a decrease in the ratio of α-myosin heavy chain (*MYH6*) to β-myosin heavy chain (*MYH7*), was observed only when cells were treated with ISO+sFRP1. *NPPA* increased in both sFRP1 ($p=0.0379$) and ISO+sFRP1-treated cells ($p<0.0001$), *NPPB* increased in ISO ($p<0.0001$) and ISO+sFRP1-treated cells ($p<0.0001$), while *MYH6/MYH7* decreased in response to sFRP1 ($p<0.0001$) and ISO+sFRP1 treatments ($p=0.0142$) (**Fig.**1a-c). sFRP1 expression increased in cells treated with ISO+sFRP1 ($p=0.0111$) (**Fig.**1d). Furthermore, the increase in sFRP1 gene expression in ISO+sFRP1-treated cells positively correlated with *NPPA* ($p=0.0004$) and *NPPB* expression ($p<0.0001$) and negatively correlated with *MYH6/MYH7* ($p<0.0001$) (Supp.**Fig.**1). These results suggest that a combination of ISO and sFRP1 promotes pathological remodeling *in vitro*.

sFRP1 and ISO treatment promotes cardiac dysfunction and dilation in a young rodent model

To further validate the translational relevance of the *in vitro* model, we tested the effect of ISO+sFRP1 *in vivo*. Rats were injected with ISO and/or sFRP1 intraperitoneally for 2 weeks (**Fig.**2a). Rats injected with ISO+sFRP1 had significantly reduced EF ($p<0.0001$)

when compared to vehicle-treated control rats, as well as when compared to rats injected solely with ISO (p=0.0316) or sFRP1 (p<0.0001) (**Fig.**2b). Echocardiogram findings also showed that left ventricular volume in systole (LV vol(s)) increased in ISO+sFRP1-treated rats compared to vehicle-treated controls (p=0.0002), ISO-treated rats (p=0.0306) or sFRP1-treated rats (p=0.0006) (**Fig.**2c). Similarly, left ventricular internal diameter in systole (LVID(s)) increased in ISO+sFRP1 rats compared to vehicle-treated controls (p<0.0001), ISO-treated rats (p=0.0334) or sFRP1-treated rats (p<0.0001) (**Fig.**2d). There were no significant differences in left ventricular anterior and posterior wall thickness for any of the treated groups (Supp Fig.2a, b). Diastolic parameters, LV vol(d) and LVID(d), followed the same trend as systolic parameters (Supp Fig**.**3a, b). Morphometric data showed a significant increase in whole heart to body weight/tibial length and LV weight to body weight/tibial length in ISO+sFRP1 rats compared to vehicle-treated controls (Supp.Fig.3c, d). Functional alterations were not restricted to male animals; changes were also observed in females (Supp.Fig.3e).

As in the *in vitro* expression studies, *NPPA* expression increased in sFRP1- (p=004) and ISO+sFRP1-treated rats (p=0.0035) compared to vehicle-treated controls (Supp. Fig 4a). However, *NPPB* expression only increased in sFRP1-treated rats (p=0.0011) and not in response to ISO+sFRP1 treatment (Supp.Fig.4b), which is also observed in paediatric iDCM[6,24]. *MYH6/MYH7* ratio decreased in both sFRP1 (p=0.0272) and ISO+sFRP1 rats (p=0.049) (Supp.Fig.4c). A simple linear regression was performed to evaluate the relationship between pathological cardiac remodeling, evidenced by reactivation of the FGP, and ejection fraction. We found that the relative expression of *NPPA*, but not *NPPB*, was significantly correlated with a decrease in EF (p=0.0039)

(Supp.Fig.5a, b), whereas the ratio of *MYH6/MYH7* trended towards a positive correlation (higher *MYH6/MYH7* correlated with higher EF) (p=0.0825) (Supp.Fig.5c). These results, together with the *in vitro* data, provide evidence that ISO+sFRP1 promotes pathological remodeling *in vitro* and cardiac dysfunction associated with left ventricular dilation *in vivo.*

To investigate the translational significance of the rat ISO+sFRP1 DCM model, we investigated cardiac mRNA and serum sFRP1 levels in rats relative to our published data in human paediatric DCM patients[7,24]. We observed a significant increase in cardiac sFRP1 mRNA levels in ISO+sFRP1 rats (p=0.0003) (Supp.Fig**.**6a) that was negatively correlated with EF (p=0.0121) (Supp.Fig.6B). Moreover, levels of sFRP1 in the serum of ISO+sFRP1 rats were significantly higher than vehicle-treated controls (Supp.Fig.6c) (p=0.0146). There was a trend to negative correlation when analyzing levels of serum circulating sFRP1 and EF (p=0.0888) in rats (Supp.Fig.6d). The observed increase in rat cardiac and serum sFRP1 levels was comparable to our previously published human data[7].

ISO+sFRP1 promotes increased stiffness in the absence of myocyte hypertrophy or fibrosis.

We previously showed that DCM serum or sFRP1 treatment promotes stiffness in NRVMs assessed by atomic force microscopy (AFM)[7]. To further explore if sFRP1 promotes stiffness *in vivo*, we investigated myocardial stiffness in rats. As shown in **Fig.**2e, ISO+sFRP1 promoted a significant increase in LV stiffness when compared to vehicle-treated control rats (p=0.02). Stiffness is specific to cardiac dysfunction as

changes in myocardial stiffness were not observed in rats treated with ISO only or sFRP1 only (Supp.Fig.7a-d). Importantly, we tested stiffness in the LV of children with DCM and show that stiffness is increased when compared to NF healthy controls (p=0.0176) (**Fig.**2f).

We and others previously showed that paediatric DCM patients have minimal fibrosis and lack myocyte hypertrophy[4,15]. Compared to vehicle-treated controls, ISO+sFRP1 rats did not exhibit increased fibrosis, as determined by Masson's trichrome staining (Supp.Fig.8a). Additionally, RT-qPCR analysis of the rat LV tissue demonstrated no significant upregulation of profibrotic genes, including *COL1A1, COL3A1, Galectin-3, TGFB1*, *TGFB2* and *TIMP1-4* (Supp.Fig.8b). Furthermore, myocyte hypertrophy was not observed in ISO+sFRP1 rats compared to controls (Supp.Fig.8c).

Notch signaling is altered in ISO+sFRP1 rats and in paediatric DCM hearts.

To better understand the pathophysiology of ISO+sFRP1-mediated DCM and identify the mechanisms underlying the disease, we performed bulk RNA sequencing analysis of the LV of rats treated with ISO and/or sFRP1 compared to vehicle-treated controls (n=6/group) (**Fig.**3a). Of the 14,350 genes identified, there were 286 differentially expressed genes (DEGs) ($p<0.05$) in ISO+sFRP1 rats compared to vehicle-treated controls (113 up-regulated and 173 down-regulated) (Supp.Table 2). Unsupervised hierarchical clustering separated control and ISO+sFRP1 treatment groups based on the gene expression profile. Unsupervised hierarchical cluster heatmaps of the top 50 DEGs in ISO+sFRP1- (**Fig.**3b), sFRP1- or ISO-treated rats (supp.Fig.9a, b) compared to vehicle-treated controls were generated and showed a clear separation between

individual groups and control. Pathways were analyzed using the identified significantly upregulated or downregulated genes. Pathway analysis of upregulated genes highlighted Notch signaling pathway as one of the main dysregulated pathways associated with upregulated genes uniquely enriched in response to ISO+sFRP1 compared to controls (**Fig.**3c left). WNT/β-catenin signaling was the 2nd top pathway for all dysregulated DEGs in ISO+sFRP1 rats (**Fig.**3c right). Pathway analysis was also done for downregulated genes (Supp.Fig.9c), and for ISO- or sFRP1-treated rats (Supp.Fig.9f, g). The WNT/β-catenin signaling pathway was significantly dysregulated in sFRP1-treated rats while mitochondrial organization pathways were dysregulated in ISO-treated rats (Supp. Fig. 9d, e)

Importantly, in our prior investigations of explanted paediatric iDCM hearts, we identified changes in gene expression that suggested alterations in the Notch and WNT pathways[24]. To investigate commonalities in hearts from children with DCM and our rat model, we assessed similarities between DEGs from ISO+sFRP1 rats, paediatric DCM hearts, and from our previously published data on paediatric DCM serum-treated NRVMs[7]. Transcriptomic analysis revealed a substantial overlap in DEGs in the LV tissue of ISO+sFRP1-treated rats and human DCM hearts or serum-treated cells. Notably, 96% of DEGs in the LV tissue of ISO+sFRP1-treated rats were also observed in the human DCM heart (65% unique only to human LV DEGs, 31% shared between human LV and rat LV DEGs with only 4% DEGs unique to rats) (Supp.Fig**.**10a). Additionally, 43% of DEGs were common between the LV tissue of ISO+sFRP1-treated rats and NRVMs treated with human DCM serum (57% unique to NRVMs treated with human DCM serum DEGs, 1% shared between NRVMs treated with human DCM

serum DEGs and rat LV DEGs with 42% DEGs unique to rats) (Supp.Fig.10b). Again, Notch signaling was one of the top dysregulated pathways associated with commonly upregulated genes in DCM serum-treated NRVMs and LV tissue of ISO+sFRP1-treated rats (Supp.Fig.10c).

Single-nuclei RNA sequencing (snRNA-seq) identifies activation of Notch and β-catenin signaling in response to ISO+sFPR1

To further characterize the cell types and biological mechanisms altered at the individual cellular level, we performed single-nuclei RNA sequencing of LV tissue from ISO and/or sFRP1, and vehicle-treated control rats (n=3/group). A total of 9,214 nuclei in control, 11,588 nuclei in ISO-, 13,758 nuclei in sFRP1-, and 11,127 in ISO+sFRP1-treated rats were identified after cells were pooled. Clusters were annotated based on canonical cell marker expression (supp. Table3.1). We assessed the distribution of cell-type annotated nuclei across all samples and identified 26 transcriptionally distinct cell-type clusters marked by canonical gene markers (**Fig.**3d)[22,25]. A sub-analysis of ventricular cardiomyocytes identified eight different sub-clusters (Supp. Fig**.** 11a). Pathway analysis of dysregulated DEGs in the ISO+sFRP1 ventricular cardiomyocyte subcluster 2 (the cluster with the most relative proportion of ventricular cardiomyocytes) suggests activation of Notch signaling as one of the top dysregulated pathways, and *CTNNB1* (β-catenin) as one of the top transcription factors predicted to control expression of upregulated genes (**Fig.**3e, Supp.Table3.2). Additionally, pathway analysis suggests extracellular matrix (ECM) proteoglycan enrichment as the top dysregulated pathway in subcluster 6 (cluster with the 2nd most relative proportion of ventricular cardiomyocytes), and *Notch1* as one of the top transcription factors predicted

to control expression of dysregulated genes (**Fig.**3f, Supp.Table3.3). Pathways analysis was also performed on the DEGs of the stromal cell types such as fibroblast, pericytes and endothelial cells which further identifies alterations in ECM proteoglycans (Supp. Fig**.** 11b-d).

Levels of Notch change *in vivo*, *in vitro* and in human DCM hearts.

To further explore Notch signaling dysregulation in DCM, we investigated levels of Notch-target genes and Notch intracellular domain (NICD), the constitutively active form of Notch1, in the different models. We found increased expression of Notch target genes, which was associated with increased nuclear and cytoplasmic NICD. NICD protein was increased in cytoplasmic (p=0.0013) and nuclear (p=0.0143) fractions of paediatric DCM hearts (**Fig.**4a,b), in cytoplasmic (p=0.0053) and nuclear fractions (p=0.0086) of ISO+sFRP1 rat hearts (**Fig.**4c,d), and in cytoplasmic (p=0.0371) and nuclear (p =0.0119) fractions of ISO+sFRP1-treated NRVMs (**Fig.**4e,f). In parallel, we also observed increased expression of Notch-target genes; *Hey1*, was upregulated in paediatric DCM hearts (1.55x, q=0.02 from RNA-seq data)[24]. *Notch1* (p=0.0398) and *HEY1* (p=0.0467) were up regulated in ISO+sFRP1 rat hearts (Supp.Fig.12 a). *Notch1* (p=0.0276) together with the expression of Notch target genes *HEY1* (p=0.0006), *HEY2* (p=0.0124), *HES1* (p=0.0361) and *HEYL* (p=0.0436) were increased in NRVMs treated with ISO+sFRP1 compared to vehicle-treated controls (Supp.Fig.12 b). There was no increase in expression of other Notch receptor genes such as Notch2-4 (Supp.Fig.12c). Expression of *Notch 1* and Notch-target genes in ISO or sFRP1-treated NRVMs did not change (Supp.Fig.13a-e).

Levels of β-catenin change *in vivo*, *in vitro* and in human DCM hearts

sFRP1 is known to modulate the WNT/β-catenin pathway in a context-dependent manner[26]. As shown in **Fig.** 3 our transcriptomic data strongly also suggested the activation of the WNT/β-catenin signaling in ISO+sFRP1-treated rats, which is in agreement with our published explanted paediatric DCM heart data[24]. We found higher levels of β-catenin in the cytoplasmic (p=0.0013) and nuclear (p=0.0433) fractions in DCM hearts (**Fig.**5a,b), in the cytoplasmic (p=0.0099) and nuclear fractions (p-value=0.0191) of ISO+sFRP1 rat hearts (**Fig.5**c,d), and in the cytoplasmic (p=0.0101) and nuclear fractions (p=0.0039) of ISO+sFRP1-treated NRVMs (**Fig.5**e,f). Additionally, we also observed an increase in expression of *CTNNB1* (p=0.0263) in ISO+sFRP1 rats and ISO+sFRP1-treated NRVMs (p=0.0460) (Supp.Fig.14a, b). Similar to what we observed when evaluating Notch signaling, the increase in *CTNNB1* levels was unique to ISO+sFRP1-treated NRVMs and was not observed in response to ISO or sFRP1. (Supp.Fig.14c)

β-catenin contributes to Notch activation in ISO+sFRP1-treated cells

Others have reported an interplay between Notch and β-catenin signaling[27,28]. We next evaluated the contribution of β-catenin to Notch activation and vice versa. siRNA-mediated down-regulation of *CTNNB1* in ISO+sFRP1-treated cells prevented ISO+sFRP1-mediated activation of Notch target gene expression by blunting expression of *HEY1* (p<0.0001), *HEY2* (p=0.0026), *HES1* (p=0.0167) and *HEYL* (p=0.0401) (**Fig.**6a). Additionally, siRNA for *CTNNB1* also prevented activation of the FGP by ISO+sFRP1 by blunting the increase in expression of *NPPA* (p=0.0063) and *NPPB*

(p=0.0003), and by increasing the ratio of *MYH6/MYH7* (p=0.0446) (**Fig.**6b). siRNA for *CTNNB1* also reduced the cytoplasmic (p=0.0041) (**Fig.**6c) and nuclear (p=0.0063) (**Fig.**6d) increase of NICD by ISO+sFRP1. The effect of si-CTNNB1 on β-catenin levels is shown in **Fig**.7 c, d.

Notch antagonism prevented pathological remodeling *in vitro* and cardiac dysfunction associated with dilation *in vivo*

We also tested the effect of DAPT, a γ-secretase inhibitor known for reducing the levels of NICD, on β-catenin levels and activation of the FGP. DAPT, as expected, prevented or decreased the activation of Notch target genes *HEY1* (p<0.0001), *HEY2* (p=0.0004), *HES1* (p<0.0001) and *HEYL* (p<0.0001) by ISO+sFRP1 (**Fig.**7a). We next tested whether Notch inhibition affected activation of the FGP. As shown in **Fig.** 7b. DAPT prevented the reactivation of FGP by ISO+sFRP1 by blunting the increased expression of *NPPA* (p=0.025), and *NPPB* (p=0.0014), and by increasing the ratio of *MYH6/MYH7* (p=0.007). Additionally, DAPT prevented ISO+sFRP1-mediated increase in cytoplasmic (p=0.0487) (**Fig.**8c) and nuclear (p=0.0385) (**Fig.**8d) β-catenin. DAPT also prevented the increase in *CTNNB1* gene expression by ISO+sFRP1 (p=0.008) (**Fig.**8e). These data support the premise that the co-activation of Notch and β-catenin promotes pathological remodeling.

Lastly, we investigated the role of DAPT in preventing cardiac dysfunction associated with ventricular dilation in our ISO+sFRP1 *in vivo* model **(Fig.8**a**)**. DAPT prevented the reduction of EF by ISO+sFRP1 (p=0.0048) and trended towards inhibiting the increase

in LV vol(s) (p=0.088) and LVID(s) (p=0.0935) (**Fig.** 8b-d). Additionally, DAPT also abrogated the increase in myocardial stiffness mediated by ISO+sFRP1 (p=0.0179) (**Fig.** 8e). This increase in myocardial stiffness negatively correlated with cardiac dysfunction (p=0.0271) (**Fig.** 8f). These results suggest that Notch inhibition improves cardiac function and myocardial stiffness in our rat model.

DISCUSSION

sFRP1-mediated pathologic remodeling and cardiac dysfunction

Studies focused on the mechanisms of HF in children are lacking. Our ISO+sFRP1 rat exhibits ventricular dilation, cardiac dysfunction, myocardial stiffness with minimal fibrosis, and activation of Notch-WNT signaling, closely paralleling the paediatric iDCM phenotype.

These findings suggest that sFRP1 in the presence of increased β-adrenergic stimulation (ISO) primes cardiomyocytes to revert to a fetal-like transcriptional state, which is a hallmark of maladaptive cardiac remodeling and HF and drives structural and functional cardiac dysfunction *in vivo*. Our study relied on these as canonical markers of pathological remodeling based on our prior studies and others[7,24,29]. We and others have shown that *NPPB* expression is not always elevated in paediatric DCM hearts[24] which is consistent with our findings in this model**.** Our *in vivo* model validates ISO+sFRP1 as a model of cardiac dysfunction that recapitulates several aspects of paediatric iDCM. Our model has an over 10% absolute reduction in EF which is a significant and important indicator of decline and physiological change in the hearts pumping ability relative to controls. Such declines in cardiac function in humans are

associated with increased risk of all-cause mortality[30]. The dilated chambers are one of the primary criteria for DCM and the significant increase in dilation cannot be explained by other causes. Considering we observed significant changes in Echo parameters after only 2 weeks of treatment with ISO+sFRP1, our model is likely to represent the early onset of iDCM. This allows us to investigate molecular responses to pathological insults, rather than investigating changes associated with end-stage heart failure

sFRP1 regulation of WNT signaling

sFRP1 is traditionally viewed as a WNT signaling antagonist, which reduces β-catenin levels. Our results suggest that sFRP1, in the context of β-adrenergic stimulation, acts as a WNT agonist rather than an antagonist as evidenced by the increased levels of β-catenin in ISO+sFRP1-treated cells and rats. Importantly, the increase in β-catenin levels was also observed in explanted paediatric DCM hearts. In support of our findings, other models of cardiac disease (such as myocardial infarction, cardiac fibrosis and HF) have highlighted the role of sFRP1 in activating WNT signaling in response to cardiac injury[31].

Classically, sFRP1 inhibition of WNT signaling occurs relatively rapidly. Within the first 1-6 hours of treatment, sFRP1 inhibits WNT signaling by directly binding to WNT ligands or to frizzled receptors[32]. However, prolonged exposure and/or increased concentration of sFRP1 can promote β-catenin stabilization and WNT signaling activation[33]. Our results agree with these findings, as initial exposure to ISO+sFRP1 did not increase β-catenin levels (not shown), but persistent (72 hours) exposure increased levels of β-catenin in cardiomyocytes. The mechanisms associated with sFRP1-

mediated stabilization of β-catenin are unclear; sFRP1 may directly form complexes with frizzled receptors, possibly mimicking the effects of WNT ligands or displacing inhibitory interactions, thus activating downstream signaling[34]. Furthermore, it has been proposed that the duration or levels of exposure to sFRP1 may stabilize certain WNT ligands or alter receptor dynamics to enhance β-catenin accumulation[33].

Our results also suggest a context-dependent function of sFRP1, in which sFRP1 may differentially modulate WNT signaling under adrenergic stress. In cancer, chronic adrenergic stress has been shown to promote sFRP1 secretion, enhancing tumor growth through β-catenin activation[33]. Hence targeting sFRP1 has been explored as a potential therapeutic target for patients with adenocarcinoma[35]. Our findings extend these observations by demonstrating that simultaneous β-adrenergic stimulation and WNT pathway modulation can synergistically trigger maladaptive gene expression patterns and cardiac dysfunction, which may be unique to the paediatric population. In this context, ISO appears to act as a modulator of the response to sFRP1 and may modify the cellular context, allowing WNT signaling components to become activated despite the presence of a known antagonist, perhaps through non-canonical or compensatory mechanisms.

The interplay between Notch-WNT signaling

Using transcriptomic data from our animal model, our data on molecular alterations in paediatric iDCM hearts and serum-treated NRVMs, we explored molecular pathways commonly altered in all models[7,24]. These data highlight activation of Notch and WNT signaling. The WNT/β-catenin pathway has a biphasic role in cardiac development and

differentiation, promoting cardiac differentiation before gastrulation and inhibiting cardiac development after gastrulation[26]. Additionally, although stabilizing β-catenin promotes proliferation of mammalian cardiomyocytes[36], it is also required for stress-induced cardiac hypertrophy[37]. These studies highlight the complexity of WNT/β-catenin signaling in the heart. In our study, we show that WNT/β-catenin contributes to a pathological phenotype, suggesting the activation of this pathway in post-natal hearts is associated with maladaptive remodeling and cardiac dysfunction.

Notch signaling is fundamentally involved in cell-cell communication and has been implicated in cardiac development, function and cardiac birth defects[38]. Notch target genes contribute to cardiac development and disease[39], and aberrations in the Notch signaling pathway are associated with congenital heart defects[40]. In addition, Notch signaling is activated after cardiac injury[41], and promotes cardiac regeneration[42], and cellular stiffness[43]. These suggest that Notch might be beneficial in regenerative, compliant environments such as the developing heart, but potentially detrimental in stiff, non-regenerative conditions such as the postnatal heart.

In the heart, Notch and WNT pathways are tightly regulated during embryogenesis, where they coordinate cardiac progenitor specification and morphogenesis[42]. However, in disease states, their reactivation often contributes to maladaptive remodeling[44]. Previous studies have shown that WNT/β-catenin signaling can enhance Notch pathway activation through direct transcriptional regulation of Notch ligands[27,28] while Notch signaling has been reported to modulate β-catenin stability and nuclear translocation[45]. This bidirectional crosstalk may underlie the robust transcriptional and protein response

we observed in our data. Interestingly, in our model, we observed an expansion of cardiomyocyte cluster 2 in ISO+sFRP1 hearts. In this cluster, there is an upregulation of Notch signaling, and *CTNNB1* is predicted to be one of the top transcriptional regulators, supporting our findings that ISO+sFRP1 treatment results in WNT/Notch activation. Thus, the expansion of ventricular cardiomyocyte nuclei in cluster 2 may reflect both a compensatory survival mechanism and a shift toward a transcriptionally dysregulated state driven by concordant Notch-WNT pathway synergy. In congruence, ventricular cardiomyocyte cluster 6 projects *Notch1* as one of the top transcription factors predicted to control expression of upregulated genes. This suggests that one cluster may be more β-catenin-regulated and the other Notch-regulated.

Our observation that both pathways are upregulated in ISO+sFRP1-treated cells, rats, and human DCM hearts suggests a cooperative role in driving pathological gene expression programs associated with cardiac dysfunction and ventricular dilation *in vivo*. These findings support a model in which combined β-adrenergic stimulation and increased WNT signaling activate Notch–WNT signaling, contributing to sustained pathological remodeling and cardiac dysfunction.

Notch as a potential therapeutic target in paediatric iDCM*.*

We also show that inhibiting Notch/WNT signaling prevents pathological remodeling. Modulating these pathways could offer age-specific strategies for paediatric HF that differ from adult therapies, especially in diseases like DCM. DAPT, a γ-secretase inhibitor, has shown promise as a potential therapeutic target for many conditions

ranging from cancer to cardiovascular diseases. DAPT promotes cardiac reprogramming and has been suggested as a potential therapeutic option for cardiac regeneration[46]. In this study, we show that DAPT prevents cardiac dysfunction in ISO+sFRP1-treated rats. These findings provide not only mechanistic insight into DCM in children but also a potential therapeutic target for paediatric DCM.

Cardiac stiffness as a characteristic of paediatric DCM

Additionally, our *in vivo* model recapitulates other aspects of paediatric iDCM, such as no difference in cardiac *NPPB* levels, minimal fibrosis or lack of myocyte hypertrophy[15,24]. While fibrosis was not observed in our model, we detected an increase in myocardial stiffness, which recapitulates our prior *in vitro* studies in cells treated with sFRP1[7]. Although the lack of fibrosis might also be a result of the early onset of the disease and acute nature of this model, the increase in stiffness in the absence of fibrosis highlights that these two processes can be independently regulated. Notably, both WNT and Notch signaling have been implicated in the regulation of extracellular matrix dynamics and fibroblast activation in adult cardiac fibrosis[47]; however, in paediatric iDCM, our transcriptomic data suggest these pathways may instead contribute to cardiomyocyte-intrinsic changes and ECM remodeling resulting in stiffness in the absence of classical interstitial fibrosis. The enrichment of ECM pathways in our rat model aligns with this observation and supports the idea that paediatric iDCM may involve dynamic ECM dysregulation without overt fibrotic conversion. Also, ECM remodeling in the absence of overt fibrosis may represent a unique pathogenic mechanism underlying paediatric iDCM. Although ECM remodeling and myocardial

stiffness have been detected in the hearts of children with iDCM[5,26], it is possible that modifications of sarcomeric proteins have an impact on stiffness which deserves further investigations. These analyses, in conjunction with myofibril stiffness investigations, will be part of future studies. Taken together, our findings suggest myocardial stiffness as an important contributor to paediatric iDCM and support WNT and Notch signaling pathways as important drivers of the disease in children.

CONCLUSION

Our study identified a novel paradigm in the investigations of paediatric iDCM that consists of a combined activation of WNT and Notch pathways. paediatricpaediatricMechanistically, *in vitro* inhibition of Notch and β-catenin signaling prevented pathological remodeling, and *in vivo* Notch inhibition improved cardiac function and myocardial stiffness. These results emphasize the relevance of our model for studying paediatric-specific mechanisms of HF and suggest that targeting the Notch–WNT axis could offer new therapeutic opportunities in paediatric DCM.

LIMITATIONS

(1) This study focused on a young model of disease and its relationship to the paediatric heart. Adults were not included in our analysis. (2) Our model of disease represents an early onset model of iDCM as the intent is to investigate disease mechanisms prior to end stage HF priorpaediatricpaediatric to puberty. (3) Although our studies suggest Notch inhibition may be a sound approach to prevent the disease process, the effect of inhibiting β-catenin is yet to be investigated. (4) The current study focused on the

interplay between β-catenin and Notch. However, other pathways identified in our transcriptomic data may be relevant and can be further explored in future studies.

Author contributions

OON performed experiments, data analysis and interpretation, manuscript writing and editing. ER performed experiments, data analysis and manuscript writing. JG performed experiments and data analysis. AKF performed statistical and bioinformatics analyses. CC performed experiments. LHL performed experiments. MPAB performed data analysis. BP performed experiments and guided AFM analysis. SDM was involved in experimental design, project supervision, clinical data interpretation, and manuscript writing and editing. BLS was involved in experimental design, project supervision, data interpretation, and manuscript writing and editing. CCS conceptualized the study, was involved in experimental design, data analysis and interpretation, manuscript writing and editing. All authors reviewed and approved the manuscript.

Acknowledgments

We would like to acknowledge the Heart Transplant Team at Children's Hospital Colorado, the University of Colorado hemodynamics core, especially Elizabeth Hardy, and the Integrated Physiology Program at the University of Colorado, particularly Dr. Mary Weiser-Evans, the program Director.

Sources of Funding

This work was supported by NIH K24HL150630 (to CCS), the Colorado CTSA Grant (UL1 TR002535), NIH R01HL156670 (to SDM, BLS, CCS), the Jack Cooper Millisor

Chair in Paediatric Heart Disease (to SDM), American Heart Association (AHA) supplement to promote diversity in science (24DIVSUP1281949) (to OON), AHA predoctoral fellowship (25PRE1375864) (to OON), NIH K25HL148386 (to BP), the Ludeman Family Center for Women's Health Research seed grant (to BP), AHA 23CDA1052411 (to BP) and the generous grants of John Patrick Albright (to BP).

Disclosure of interest

None of the authors have a conflict of interest

Data Availability

The datasets supporting the current study including raw, processed and metadata of RNA sequencing will be made publicly available in NCBI GEOdatabase upon acceptance of the manuscript for publication.

References

1. Loss KL, Shaddy RE, Kantor PF. Recent and Upcoming Drug Therapies for Paediatric Heart Failure. *Front Pediatr*. 2021;9:11. doi:10.3389/FPED.2021.681224
2. Shaddy RE, Curtin EL, Sower B, et al. The paediatric randomized carvedilol trial in children with chronic heart failure: Rationale and design. *Am Heart J*. 2002;144(3):383-389. doi:10.1067/mhj.2002.124402
3. Quiat D, Witkowski L, Zouk H, Daly KP, Roberts AE. Retrospective Analysis of Clinical Genetic Testing in Paediatric Primary Dilated Cardiomyopathy: Testing Outcomes and the Effects of Variant Reclassification. *J Am Heart Assoc*. 2020;9(11). doi:10.1161/JAHA.120.016195
4. Patel MD, Mohan J, Schneider C, et al. Paediatric and adult dilated cardiomyopathy represent distinct pathological entities. *JCI Insight*. 2017;2(14). doi:10.1172/JCI.INSIGHT.94382
5. Taegtmeyer H, Sen S, Vela D. Return to the fetal gene program: A suggested metabolic link to gene expression in the heart. *Ann N Y Acad Sci*. 2010;1188:191. doi:10.1111/J.1749-6632.2009.05100.X
6. Nyarko OO, Sucharov CC. The secretome as a biomarker and functional agent in heart failure. *J Cardiovasc Aging 2023;3:27*. 2023;3(3):N/A-N/A. doi:10.20517/JCA.2023.15

7. Jeffrey DA, da Silva JP, Garcia AM, et al. Serum circulating proteins from paediatric patients with dilated cardiomyopathy cause pathologic remodeling and cardiomyocyte stiffness. *JCI Insight*. 2021;6(19). doi:10.1172/JCI.INSIGHT.148637
8. Liang CJ, Wang ZW, Chang YW, Lee KC, Lin WH, Lee JL. SFRPs Are Biphasic Modulators of Wnt-Signaling-Elicited Cancer Stem Cell Properties beyond Extracellular Control. *Cell Rep*. 2019;28(6):1511-1525.e5. doi:10.1016/J.CELREP.2019.07.023
9. Gao J, Fan L, Zhao L, Su Y. The interaction of Notch and Wnt signaling pathways in vertebrate regeneration. *Cell Regeneration 2021 10:1*. 2021;10(1):1-17. doi:10.1186/S13619-020-00072-2
10. Fre S, Pallavi SK, Huyghe M, et al. Notch and Wnt signals cooperatively control cell proliferation and tumorigenesis in the intestine. *Proc Natl Acad Sci U S A*. 2009;106(15):6309. doi:10.1073/PNAS.0900427106
11. Quillard T, Charreau B. Impact of Notch Signaling on Inflammatory Responses in Cardiovascular Disorders. *International Journal of Molecular Sciences 2013, Vol 14, Pages 6863-6888*. 2013;14(4):6863-6888. doi:10.3390/IJMS14046863
12. Lefkowitz RJ, Rockman HA, Koch WJ. Catecholamines, Cardiac β-Adrenergic Receptors, and Heart Failure. *Circulation*. 2000;101(14):1634-1637. doi:10.1161/01.CIR.101.14.1634
13. Venugopalan P, Agarwal AK. Plasma catecholamine levels parallel severity of heart failure and have prognostic value in children with dilated cardiomyopathy. *Eur J Heart Fail*. 2003;5(5):655-658. doi:10.1016/S1388-9842(03)00109-0
14. Toni LS, Garcia AM, Jeffrey DA, et al. Optimization of phenol-chloroform RNA extraction. *MethodsX*. 2018;5:599. doi:10.1016/J.MEX.2018.05.011
15. Woulfe KC, Siomos AK, Nguyen H, et al. Fibrosis and Fibrotic Gene Expression in Paediatric and Adult Patients With Idiopathic Dilated Cardiomyopathy. *J Card Fail*. 2017;23(4):314-324. doi:10.1016/J.CARDFAIL.2016.11.006
16. Sucharov CC, Dockstader K, McKinsey TA. YY1 protects cardiac myocytes from pathologic hypertrophy by interacting with HDAC5. *Mol Biol Cell*. 2008;19(10):4141-4153. doi:10.1091/mbc.E07-12-1217
17. Sucharov CC, Hijmans JG, Sobus RD, Melhado WFA, Miyamoto SD, Stauffer BL. β-Adrenergic receptor antagonism in mice: a model for paediatric heart disease. *J Appl Physiol (1985)*. 2013;115(7):979-987. doi:10.1152/JAPPLPHYSIOL.00627.2013
18. Garcia AM, Nakano SJ, Karimpour-Fard A, et al. Phosphodiesterase-5 is Elevated in Failing Single Ventricle Myocardium and Affects Cardiomyocyte Remodeling in vitro. *Circ Heart Fail*. 2018;11(9):e004571. doi:10.1161/CIRCHEARTFAILURE.117.004571
19. Peña B, Adbel-Hafiz M, Cavasin M, Mestroni L, Sbaizero O. Atomic Force Microscopy (AFM) Applications in Arrhythmogenic Cardiomyopathy. *International Journal of Molecular Sciences 2022, Vol 23, Page 3700*. 2022;23(7):3700. doi:10.3390/IJMS23073700
20. Blomberg R, Sompel K, Hauer C, et al. Tissue-engineered models of lung cancer premalignancy. *bioRxiv*. Published online March 17, 2023:2023.03.15.532835. doi:10.1101/2023.03.15.532835
21. Dobin A, Davis CA, Schlesinger F, et al. STAR: ultrafast universal RNA-seq aligner. *Bioinformatics*. 2013;29(1):15-21. doi:10.1093/BIOINFORMATICS/BTS635
22. Koenig AL, Shchukina I, Amrute J, et al. Single-cell transcriptomics reveals cell-type-specific diversification in human heart failure. *Nature cardiovascular research*. 2022;1(3):263-280. doi:10.1038/S44161-022-00028-6
23. Hao Y, Hao S, Andersen-Nissen E, et al. Integrated analysis of multimodal single-cell data. *Cell*. 2021;184(13):3573-3587.e29. doi:10.1016/J.CELL.2021.04.048
24. Tatman PD, Woulfe KC, Karimpour-Fard A, et al. Paediatric dilated cardiomyopathy hearts display a unique gene expression profile. *JCI Insight*. 2017;2(14). doi:10.1172/JCI.INSIGHT.94249

25. Amrute JM, Lai L, Ma P, et al. Defining cardiac functional recovery in end-stage heart failure at single-cell resolution. *Nature cardiovascular research*. 2023;2(4):399. doi:10.1038/S44161-023-00260-8
26. Ueno S, Weidinger G, Osugi T, et al. Biphasic role for Wnt/β-catenin signaling in cardiac specification in zebrafish and embryonic stem cells. *Proc Natl Acad Sci U S A*. 2007;104(23):9685. doi:10.1073/PNAS.0702859104
27. Kumar V, Vashishta M, Kong L, et al. The Role of Notch, Hedgehog, and Wnt Signaling Pathways in the Resistance of Tumors to Anticancer Therapies. *Front Cell Dev Biol*. 2021;9:650772. doi:10.3389/FCELL.2021.650772
28. Galceran J, Sustmann C, Hsu SC, Folberth S, Grosschedl R. LEF1-mediated regulation of Delta-like1 links Wnt and Notch signaling in somitogenesis. *Genes Dev*. 2004;18(22):2718. doi:10.1101/GAD.1249504
29. Taegtmeyer H, Sen S, Vela D. Return to the fetal gene program: A suggested metabolic link to gene expression in the heart. *Ann N Y Acad Sci*. 2010;1188:191. doi:10.1111/J.1749-6632.2009.05100.X
30. Shams P, Goyal A, Makaryus AN. Left Ventricular Ejection Fraction. *StatPearls*. Published online June 14, 2025. Accessed September 4, 2025. https://www.ncbi.nlm.nih.gov/books/NBK459131/
31. Aisagbonhi O, Rai M, Ryzhov S, Atria N, Feoktistov I, Hatzopoulos AK. Experimental myocardial infarction triggers canonical Wnt signaling and endothelial-to-mesenchymal transition. *Dis Model Mech*. 2011;4(4):469-483. doi:10.1242/DMM.006510
32. Regel I, Eichenmüller M, Mahajan UM, et al. Downregulation of SFRP1 is a protumorigenic event in hepatoblastoma and correlates with beta-catenin mutations. *J Cancer Res Clin Oncol*. 2020;146(5):1153-1167. doi:10.1007/S00432-020-03182-1/TABLES/2
33. Lin XH, Liu HH, Hsu SJ, et al. Norepinephrine-stimulated HSCs secrete sFRP1 to promote HCC progression following chronic stress via augmentation of a Wnt16B/β-catenin positive feedback loop. *J Exp Clin Cancer Res*. 2020;39(1). doi:10.1186/S13046-020-01568-0
34. Bu Q, Li Z, Zhang J, Xu F, Liu J, Liu H. The crystal structure of full-length Sizzled from Xenopus laevis yields insights into Wnt-antagonistic function of secreted Frizzled-related proteins. *Journal of Biological Chemistry*. 2017;292(39):16055-16069. doi:10.1074/JBC.M117.791756
35. Cheng LC, Chao YJ, Overman MJ, et al. Increased expression of secreted frizzled related protein 1 (SFRP1) predicts ampullary adenocarcinoma recurrence. *Scientific Reports 2020 10:1*. 2020;10(1):1-16. doi:10.1038/s41598-020-69899-8
36. Tseng AS, Engel FB, Keating MTT. The GSK-3 inhibitor BIO promotes proliferation in mammalian cardiomyocytes. *Chem Biol*. 2006;13(9):957-963. doi:10.1016/J.CHEMBIOL.2006.08.004
37. Chen X, Shevtsov SP, Hsich E, et al. The β-Catenin/T-Cell Factor/Lymphocyte Enhancer Factor Signaling Pathway Is Required for Normal and Stress-Induced Cardiac Hypertrophy. *Mol Cell Biol*. 2006;26(12):4462. doi:10.1128/MCB.02157-05
38. Ruijmbeek CWB, Housley F, Idrees H, et al. Biallelic variants in FLII cause paediatric cardiomyopathy by disrupting cardiomyocyte cell adhesion and myofibril organization. *JCI Insight*. 2023;8(17):e168247. doi:10.1172/JCI.INSIGHT.168247
39. Fischer A, Schumacher N, Maier M, Sendtner M, Gessler M. The Notch target genes Hey1 and Hey2 are required for embryonic vascular development. *Genes Dev*. 2004;18(8):901. doi:10.1101/GAD.291004
40. Niessen K, Karsan A. Notch signaling in cardiac development. *Circ Res*. 2008;102(10):1169-1181. doi:10.1161/CIRCRESAHA.108.174318/ASSET/D2E086FF-4E20-4858-A7B0-4F339541366A/ASSETS/GRAPHIC/9FF4.JPEG

41. Li Y, Hiroi Y, Liao JK. Notch Signaling as an Important Mediator of Cardiac Repair and Regeneration after Myocardial Infarction. *Trends Cardiovasc Med*. 2010;20(7):228. doi:10.1016/J.TCM.2011.11.006
42. Li H, Chang C, Li X, Zhang R. The roles and activation of endocardial Notch signaling in heart regeneration. *Cell Regeneration*. 2021;10(1). doi:10.1186/S13619-020-00060-6
43. Kretschmer M, Mamistvalov R, Sprinzak D, Vollmar AM, Zahler S. Matrix stiffness regulates Notch signaling activity in endothelial cells. *J Cell Sci*. 2023;136(2). doi:10.1242/JCS.260442/286810
44. Malekar P, Hagenmueller M, Anyanwu A, et al. Wnt signaling is critical for maladaptive cardiac hypertrophy and accelerates myocardial remodeling. *Hypertension*. 2010;55(4):939-945. doi:10.1161/HYPERTENSIONAHA.109.141127
45. Kwon C, Cheng P, King IN, et al. Notch Post-Translationally Regulates β-Catenin Protein in Stem and Progenitor Cells. *Nat Cell Biol*. 2011;13(10):1244. doi:10.1038/NCB2313
46. Abad M, Hashimoto H, Zhou H, et al. Notch Inhibition Enhances Cardiac Reprogramming by Increasing MEF2C Transcriptional Activity. *Stem Cell Reports*. 2017;8(3):548. doi:10.1016/J.STEMCR.2017.01.025
47. Docshin P, Panshin D, Malashicheva A. Molecular Interplay in Cardiac Fibrosis: Exploring the Functions of RUNX2, BMP2, and Notch. *Rev Cardiovasc Med*. 2024;25(10):368. doi:10.31083/J.RCM2510368

FIGURES LEGENDS

Figure 1. ISO+sFRP1 promotes pathological remodeling in NRVMs.

(A) RT-qPCR of *NPPA* expression in NRVMs treated with vehicle (Control), ISO, sFRP1 or ISO+sFRP1. Gene expression was normalized to 18S, and data are presented as a relative fold change to Controls. NRVMs treated with 100nM Isoproterenol (ISO) +/- 1 µg/mL human recombinant sFRP1 for 72 hours. n = 8 independent NRVM preps. All groups are log2 transformed.

(B) RT-qPCR of *NPPB* expression in NRVMs treated with vehicle (Control), ISO, sFRP1 or ISO+sFRP1. Gene expression was normalized to 18S, and data are presented as a relative fold change to Controls. NRVMs treated with 100nM Isoproterenol (ISO) +/- 1 µg/mL human recombinant sFRP1 for 72 hours. n = 8 independent NRVM preps. All groups are log2 transformed.

(C) RT-qPCR of *MYH6/7* expression in NRVMs treated with vehicle (Control), ISO, sFRP1 or ISO+sFRP1. Gene expression was normalized to 18S, and data are presented as a relative fold change to Controls. NRVMs treated with 100nM Isoproterenol (ISO) +/- 1 µg/mL human recombinant sFRP1 for 72 hours. *n* = 8 independent NRVM preps. All groups are log2 transformed.

(D) RT-qPCR of sFRP1 gene expression in NRVMs treated with ISO+sFRP1 compared to vehicle-treated controls. Gene expression was normalized to 18S, and data are presented as a relative fold change to controls. *n* = 6 independent NRVM preps.

Figure 2. DCM phenotype in ISO+sFRP1 treated rats and cardiac stiffness is increased in paediatric DCM hearts and ISO+sFRP1 rats.

(A) Schematic of injection plan, timeline and duration. Rats were treated with 0.1mg/kg/day ISO every other day for the first 5 treatments and every day for the subsequent 7 days. sFRP1 (50µg/kg/day) was co-administered with ISO (or vehicle (PBS, 0.5mM ascorbic acid).

(B) EF of neonatal rats treated with vehicle (Control), ISO, sFRP1 and ISO+sFRP1.

(C) LV vol(s) of neonatal rats treated with vehicle (Control), ISO, sFRP1 and ISO+sFRP1.

(D) LVID(s) of neonatal rats treated with vehicle (Control), ISO, sFRP1 and ISO+sFRP1. Control *n* = 20, ISO *n* = 9, sFRP1 *n* = 9, ISO+sFRP1 *n*=19. Only significant *p*-values are notated in the Figure.

(E) Elasticity/stiffness (Young's modulus) in rats treated with ISO+sFRP1 compared to controls. Quantification is shown. *n* =3 per group

(F) Elasticity/stiffness (Young's modulus) in explanted paediatric DCM hearts compared to non-failing controls. Quantification is shown. NF *n* =3, DCM *n =4*.

Only significant *P* values (p<0.05) are notated in the Figure. Fitting a mixed model, Tukey's multiple comparisons test was used for multiple comparison. Unpaired *t*-test was used for two-group analysis. Error bar denotes mean± SEM. NRVMs, neonatal rat ventricular myocytes; FGP, fetal gene program; ISO, Isoproterenol; sFRP1, secreted frizzled protein 1; EF, ejection fraction; LV vol(s), Left ventricular volume in systole; LVID. Left ventricular internal diameter in systole; LVAW(s), left ventricular anterior wall in systole; LVPW (s), left ventricular posterior wall in systole.

Figure 3. Notch and WNT signaling are predicted to be altered in ISO+sFRP1 rats and in paediatric DCM hearts via Next generation sequencing.

(A) Schematic of the experimental plan for next generation sequencing (bulk RNA-seq and Single nuclei RNA-seq.)

(B) Heatmap representing unsupervised hierarchical clustering of the top 50 significantly differentially expressed genes (DEGs) in bulk RNA sequencing. n = 6/group; Welch's t test $p < 0.05$.

(C) Pathway analysis using the 113 upregulated genes in ISO+sFRP1 vs Control rats using Reactome pathway analysis tool (left) and Hallmark pathway analysis tool (right).

(D) Representative UMAP plot from single-nuclei RNA sequencing of LV tissue from Controls, ISO-, sFRP1- or ISO+sFRP1-treated rats, n = 3/group. A total of 9214 nuclei in control, 11588 nuclei in ISO-, 13758 nuclei in sFRP1-, and 11127 in ISO+sFRP1-treated rats were identified after cells were pooled. 26 distinct cell clusters were identified including 8 CMs and 5 FBs.

(E) Reactome pathway analysis using upregulated genes in Ventricular cardiomyocyte sub-cluster 2 of ISO+sFRP1 vs Control rats (left). Enrichr analysis identifies transcription factors predicted to control expression of upregulated genes in ventricular cardiomyocyte sub-cluster 2 (right).

(F) Reactome pathways analysis using upregulated genes in ventricular cardiomyocyte sub-cluster 6 of ISO+sFRP1 vs Control rats (left). Enrichr analysis identifies transcription factors predicted to control expression of upregulated genes in ventricular cardiomyocyte sub-cluster 6 (right).

Clusters were annotated into major cell populations, and the ventricular cardiomyocyte cluster was sub-clustered into eight different sub-clusters using R statistical software. Differentially expressed genes for each cluster were calculated with the FindAllMarkers function. UMAP: uniform manifold approximation and projection, CM: cardiomyocytes; FB: fibroblast; NK: Natural Killer cells; B/T: B cells and T cells. DCM, dilated cardiomyopathy; ISO-Isoproterenol, sFRP1- secreted frizzled protein 1; NRVMs, neonatal rat ventricular myocytes; LV, left ventricle.

Figure 4. Levels of NICD are increased in nuclear and cytoplasmic fractions in *vivo*, *in vitro* and in explanted human DCM hearts.

(A, B) Western blot showing increased protein levels of NICD in the cytoplasm (A) and nuclear fractions (B) of NF vs DCM human LV tissue with quantification. Cytoplasmic n=6/group, nuclear n=7/group.

(C, D) Western blot showing increased protein levels of NICD in the cytoplasm (C) and nuclear fractions (D) of ISO+sFRP1 vs vehicle-treated control rat LV tissue with quantifications. Cytoplasmic n=6/group, nuclear n=7/group.

(E, F) Western blot showing the increased protein levels of NICD in the cytoplasm (E) and nuclear fractions (F) of ISO+sFRP1 vs vehicle-treated NRVMs with quantifications. Cytoplasmic n = 4 independent NRVM preps, nuclear n = 5 independent NRVM preps. NICD. Notch Intracellular domain, NRVMs, neonatal rat ventricular myocytes.

NF, non-failing; DCM, dilated cardiomyopathy; NICD, Notch Intracellular domain. Unpaired 2-tailed t test was used in analysis. P-values are notated in each graph.

Figure 5. Levels of β-catenin are increased in nuclear and cytoplasmic fractions *in vivo*, *in vitro* and in human DCM hearts.

(A, B) Western blot showing increased protein levels of β-catenin in the cytoplasm (A) and nuclear fractions (B) of NF and DCM explanted human LV tissue with quantifications. NF, non-failing; DCM, dilated cardiomyopathy; cytoplasmic n=3/group, nuclear n=7/group.

(C, D) Western blot showing increased protein levels of β-catenin in the cytoplasm (C) and nuclear fractions (D) of ISO+sFRP1 vs vehicle-treated control rat LV tissue with quantifications. Cytoplasmic n=3/group, nuclear, n=7/group.

(E, F) Western blot showing increased protein levels of β-catenin in the cytoplasm (E) and nuclear fractions (F) of ISO+sFRP1 vs vehicle-treated NRVMs with quantifications. Cytoplasmic and nuclear fractions from n=4 independent NRVM preps.

NRVMs, neonatal rat ventricular myocytes. Unpaired 2-tailed t test was used in analysis. p-values are notated in each graph.

Figure 6. β-catenin contributes to Notch activation and inhibiting β-catenin prevents pathological remodeling in ISO+sFRP1-treated cells.

(A) RT-qPCR of Notch target gene expression in NRVMs transfected with scrambled control siRNA (scr) or siCTNNB1, and treated with vehicle (Control) or ISO+sFRP1. Expression of *Hey1, HEY2, HES1* and *HEYL* genes. Gene expression was normalized to 18S, and data are presented as a relative fold change to Controls. *n*=6 independent NRVM preps/group

(B) RT-qPCR of FGP gene expression in NRVMs transfected with scrambled control siRNA (scr) or siCTNNB1 and treated with vehicle (Control) or ISO+sFRP1. Expression of *NPPA, NPPB,* and ratio of *MYH6* to *MYH7*. Gene expression was normalized to 18S, and data are presented as a relative fold change to Controls. n=4 independent NRVM preps/group

(C, D) Western blot showing reduced protein levels of NICD in the cytoplasm (C) and nuclear fractions (D) of NRVMs treated with ISO+sFRP1 and transfected with si-CTNNB1 when compared to ISO+sFRP1-treated cells with quantifications. n=3 independent NRVM preps/group. NICD, Notch Intracellular domain, NRVMs, neonatal rat ventricular myocytes.

Figure 7. Notch contributes to β-catenin activation, and inhibiting Notch prevents pathological remodeling.

(A) RT-qPCR of Notch target gene expression (*HEY1, HEY2, HES1* and *HEYL)* in NRVMs treated with vehicle (Control), ISO+sFRP1, DAPT (20µM) or ISO+sFRP1+DAPT. Gene expression was normalized to 18S, and data are presented as a relative fold change to Controls. *n* = 7 independent NRVM preps/group

(B) RT-qPCR of FGP in NRVMs treated with vehicle (Control), ISO+sFRP1, DAPT (20µM) or ISO+sFRP1+DAPT. Gene expression was normalized to 18S, and data are presented as a relative fold change to Controls. *n* = 5 independent NRVM preps/group

(C) Western blot showing the reduced protein levels of β-catenin in the cytoplasm (C) and nuclear fractions (D) of ISO+sFRP1+DAPT or ISO+sFRP1-treated NRVMs with quantifications. *P*-values are notated in each graph. *n* = 4 independent NRVM preps/group. NRVM, neonatal rat ventricular myocytes

(E) RT-qPCR of CTNNB1 gene expression in NRVMs treated with vehicle (Control), ISO+sFRP1, DAPT (20µM) and ISO+Sfrp1+DAPT. Gene expression was normalized to 18S, and data are presented as a relative fold change to Controls. Tukey's multiple comparisons test was used for all data sets. Control, n = 4, ISO+sFRP1 n = 8, DAPT n = 4 and ISO+sFRP1+DAPT n = 7

Figure 8. Inhibiting Notch prevents cardiac dysfunction in ISO+sFRP1-treated rats.

(A) Schematic of the experimental plan for rats treated with ISO+sFRP1 +/-DAPT showing a prevention of cardiac dysfunction

(B) EF of neonatal rats treated with Control, ISO+sFRP1 and DAPT ISO+sFRP1.

(C) LV vol(s) of neonatal rats treated with Control, ISO+sFRP1 and DAPT ISO+sFRP1.

(D) LVID(s) of neonatal rats treated with Control, ISO+sFRP1 and DAPT ISO+sFRP1. Control n=13, ISO+sFRP1 n=13. DAPT+ISO+sFRP1 n=6.

(E) Elasticity/stiffness (Young's modulus) in rats treated with DAPT+ISO+sFRP1 compared to ISO+sFRP1 treated rats and controls. Quantification is shown. Control n=3, ISO+sFRP1 n=3 and DAPT+ISO+sFRP1 n=4

(F) Simple linear regression of cardiac function (EF) and stiffness (Young's modulus in kPa). EF: ejection fraction; LV vol(s), Left ventricular volume in systole; LVID. Left ventricular internal diameter in systole. Tukey's multiple comparisons test was used for all data sets. P-values are notated in the graph.

Appendices

Supplemental Material

Detailed Methods

Tables S1-S5

Supplemental figure legends

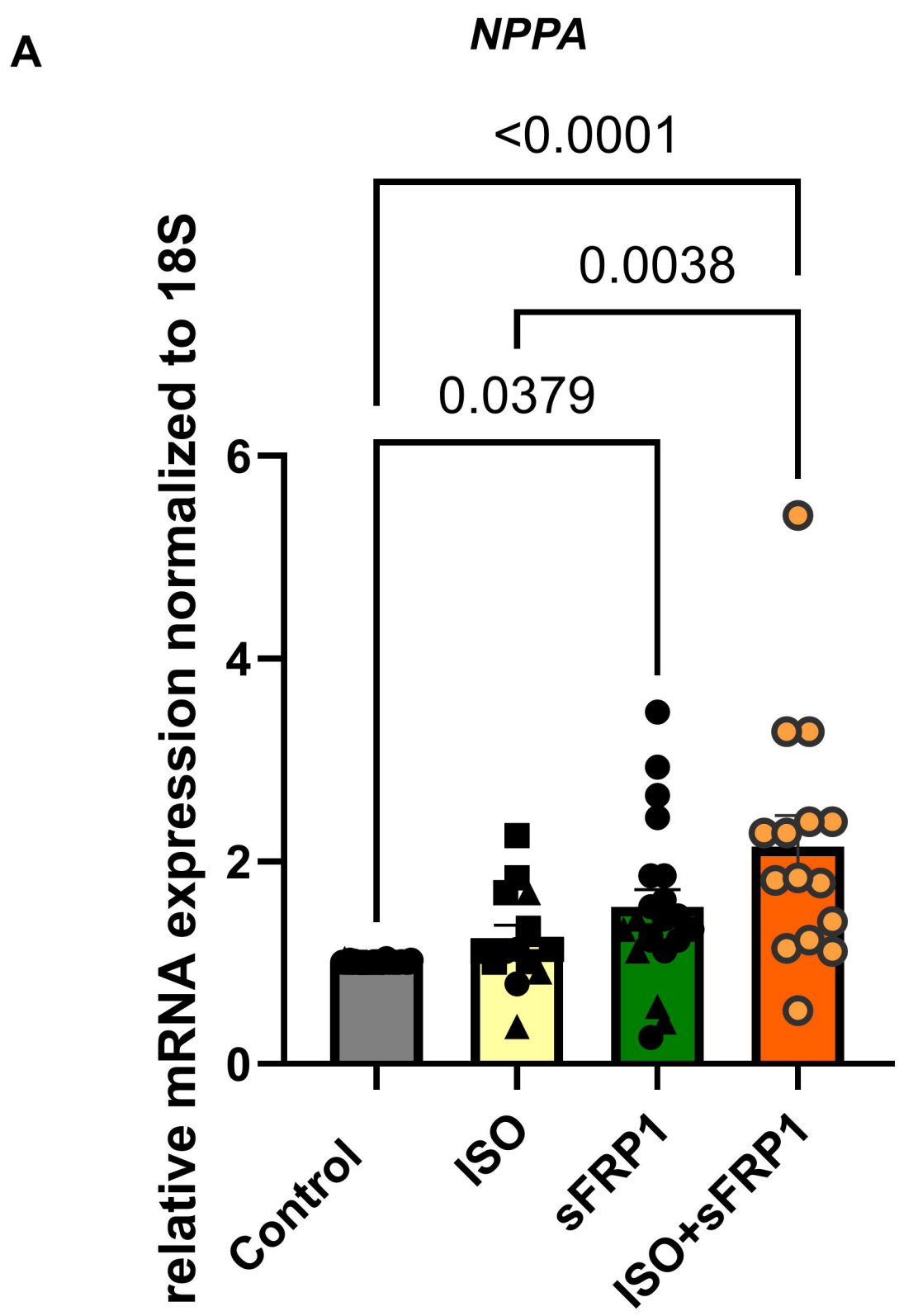
A
NPPA
<0.0001
0.0038
0.0379
relative mRNA expression normalized to 18S
0
2
4
6
Control
ISO
sFRP1
ISO+sFRP1

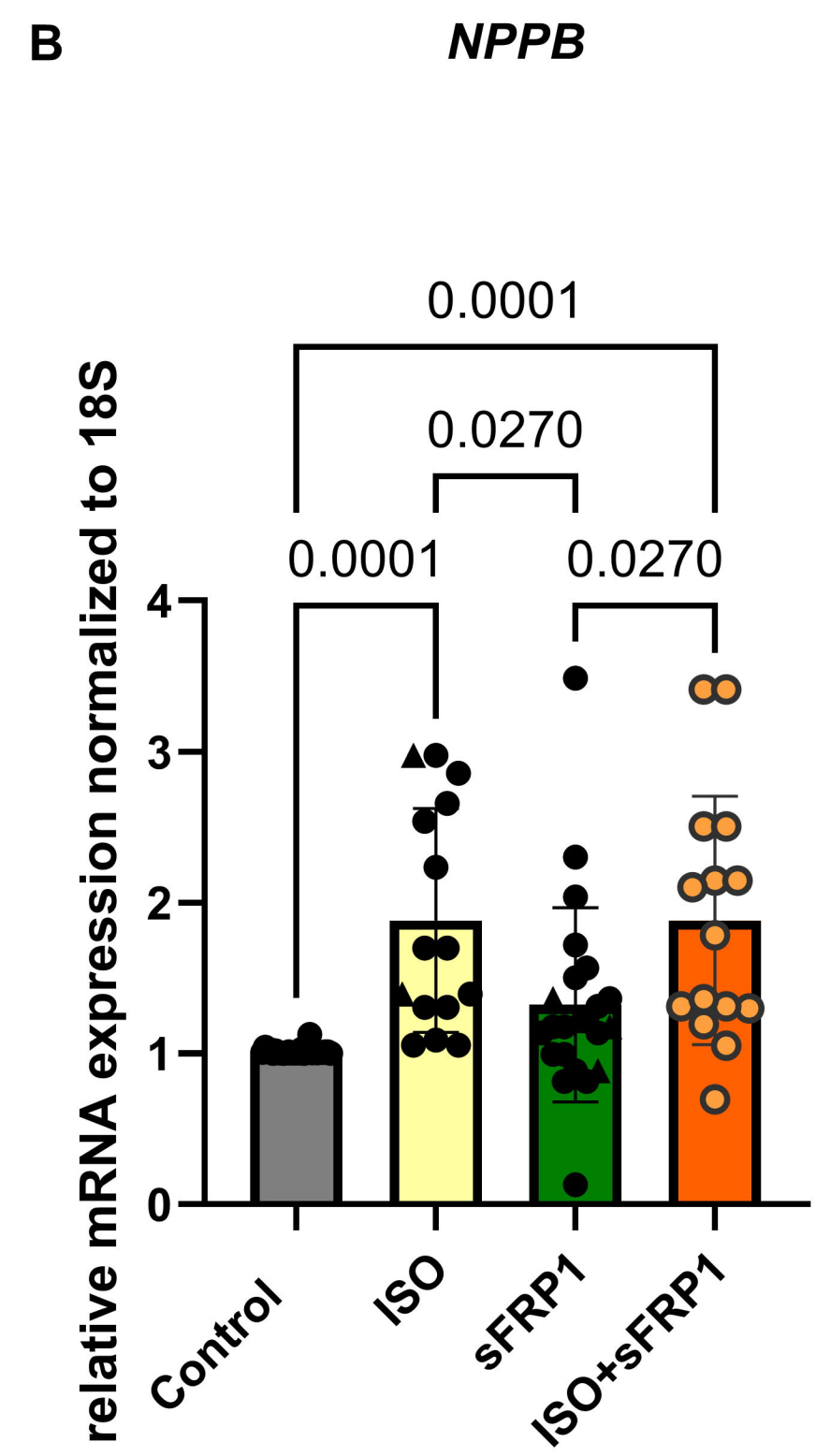
B
NPPB
0.0001
0.0270
0.0001
0.0270
relative mRNA expression normalized to 18S
0
1
2
3
4
Control
ISO
sFRP1
ISO+sFRP1

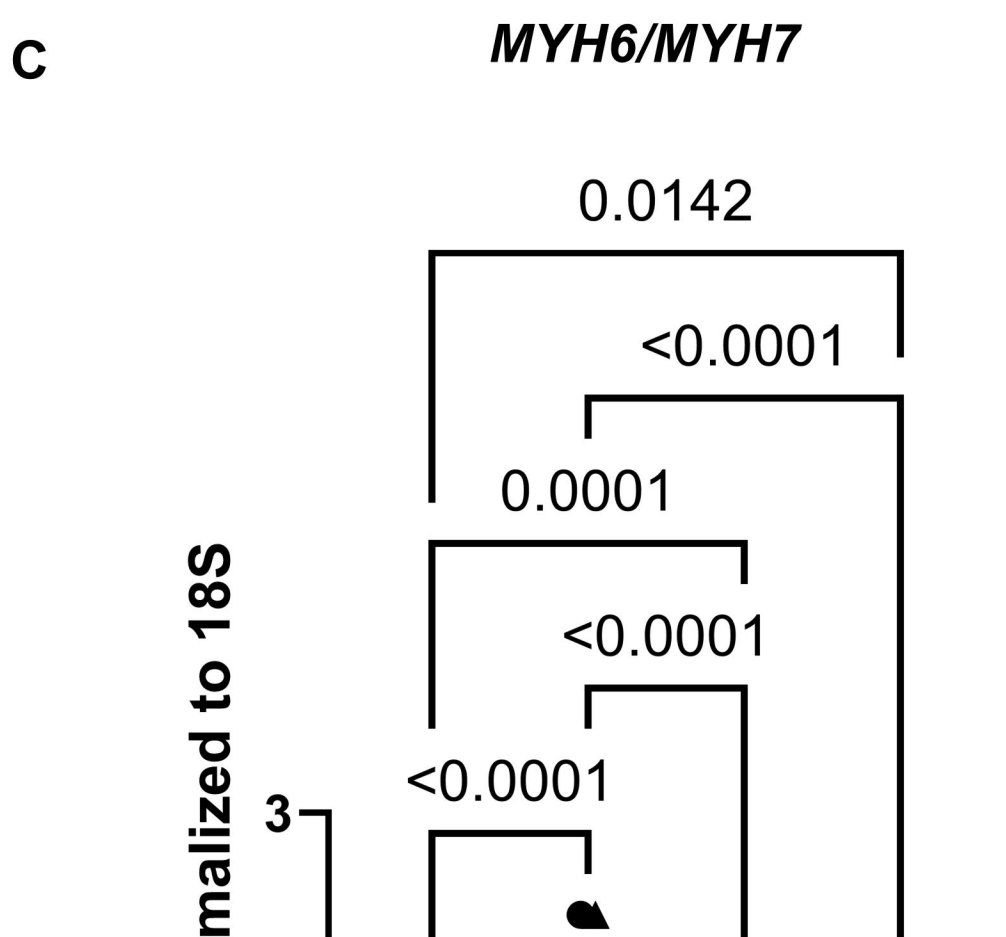
C
MYH6/MYH7
0.0142
<0.0001
0.0001
<0.0001
<0.0001
relative mRNA expression normalized to 18S
0
1
2
3
Control
ISO
sFRP1
ISO+sFRP1

D
sFRP1
0.0111
relative mRNA expression normalized to 18S
0
1
2
3
4
Control
ISO+sFRP1

FIGURE 1

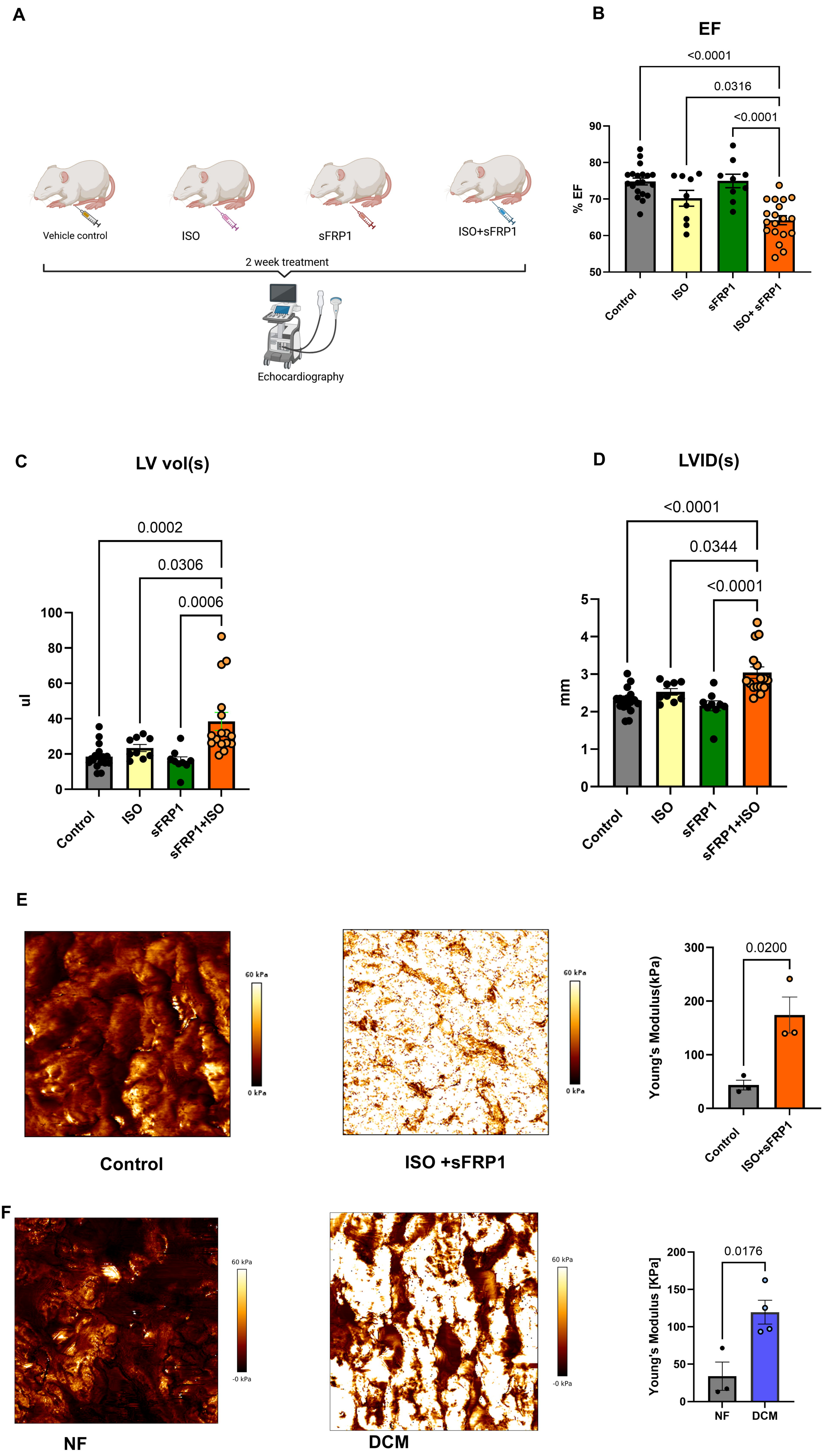
A
Vehicle control
ISO
sFRP1
ISO+sFRP1
2 week treatment
Echocardiography
B
EF
<0.0001
0.0316
<0.0001
% EF
90
80
70
60
50
Control
ISO
sFRP1
ISO+ sFRP1
C
LV vol(s)
0.0002
0.0306
0.0006
ul
100
80
60
40
20
0
Control
ISO
sFRP1
sFRP1+ISO
D
LVID(s)
<0.0001
0.0344
<0.0001
mm
5
4
3
2
1
0
Control
ISO
sFRP1
sFRP1+ISO
E
60 kPa
0 kPa
Control
60 kPa
0 kPa
ISO +sFRP1
Young's Modulus(kPa)
300
200
100
0
0.0200
Control
ISO+sFRP1
F
60 kPa
-0 kPa
NF
60 kPa
-0 kPa
DCM
Young's Modulus [KPa]
200
150
100
50
0
0.0176
NF
DCM

FIGURE 2

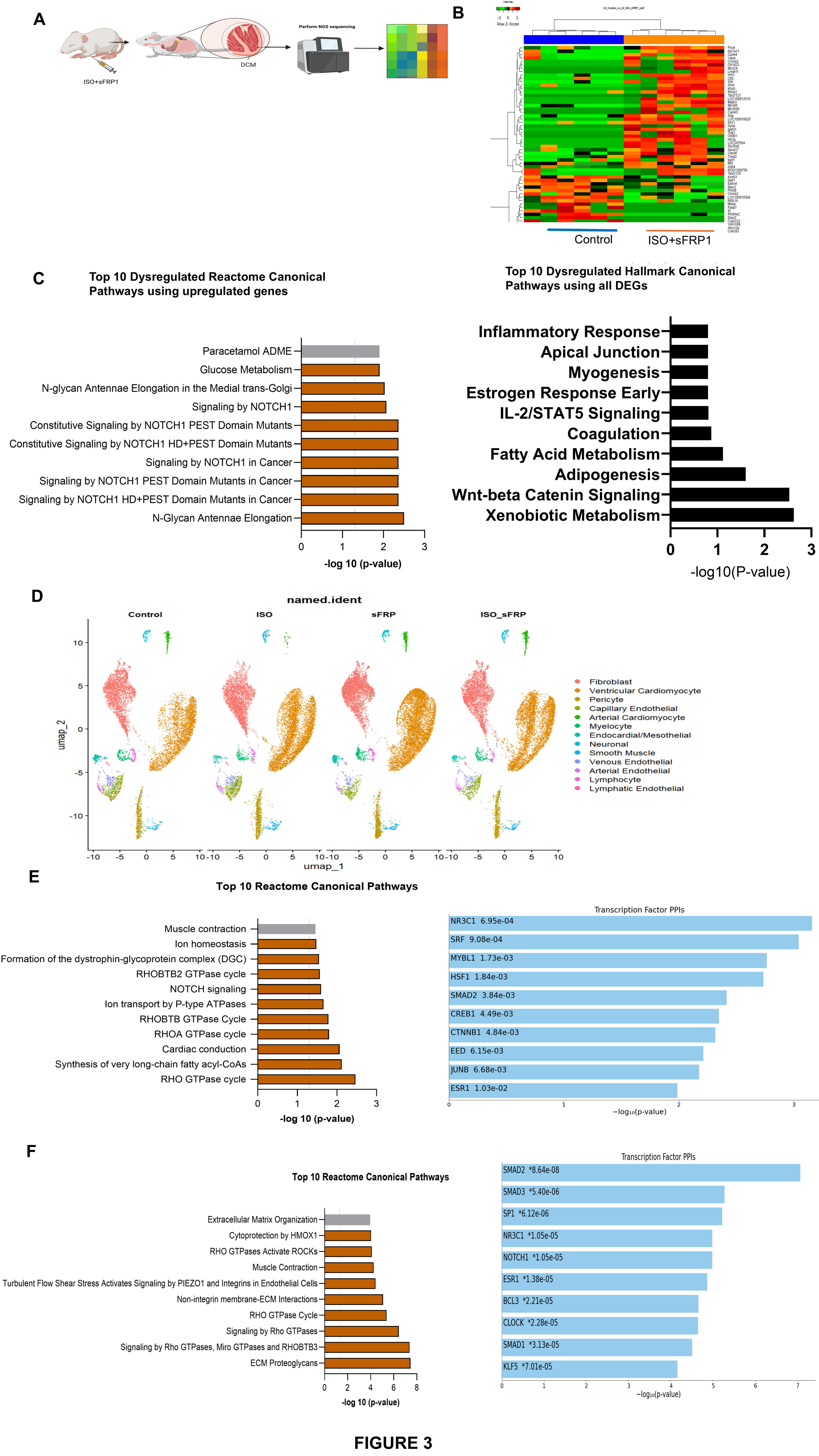
A
ISO+sFRP1
DCM
Perform NGS sequencing
B
Control
ISO+sFRP1
C
Top 10 Dysregulated Reactome Canonical Pathways using upregulated genes
Paracetamol ADME
Glucose Metabolism
N-glycan Antennae Elongation in the Medial trans-Golgi
Signaling by NOTCH1
Constitutive Signaling by NOTCH1 PEST Domain Mutants
Constitutive Signaling by NOTCH1 HD+PEST Domain Mutants
Signaling by NOTCH1 in Cancer
Signaling by NOTCH1 PEST Domain Mutants in Cancer
Signaling by NOTCH1 HD+PEST Domain Mutants in Cancer
N-Glycan Antennae Elongation
-log 10 (p-value)
Top 10 Dysregulated Hallmark Canonical Pathways using all DEGs
Inflammatory Response
Apical Junction
Myogenesis
Estrogen Response Early
IL-2/STAT5 Signaling
Coagulation
Fatty Acid Metabolism
Adipogenesis
Wnt-beta Catenin Signaling
Xenobiotic Metabolism
-log10(P-value)
D
named.ident
Control
ISO
sFRP
ISO_sFRP
umap_2
umap_1
Fibroblast
Ventricular Cardiomyocyte
Pericyte
Capillary Endothelial
Arterial Cardiomyocyte
Myelocyte
Endocardial/Mesothelial
Neuronal
Smooth Muscle
Venous Endothelial
Arterial Endothelial
Lymphocyte
Lymphatic Endothelial
E
Top 10 Reactome Canonical Pathways
Muscle contraction
Ion homeostasis
Formation of the dystrophin-glycoprotein complex (DGC)
RHOBTB2 GTPase cycle
NOTCH signaling
Ion transport by P-type ATPases
RHOBTB GTPase Cycle
RHOA GTPase cycle
Cardiac conduction
Synthesis of very long-chain fatty acyl-CoAs
RHO GTPase cycle
-log 10 (p-value)
Transcription Factor PPIs
NR3C1 6.95e-04
SRF 9.08e-04
MYBL1 1.73e-03
HSF1 1.84e-03
SMAD2 3.84e-03
CREB1 4.49e-03
CTNNB1 4.84e-03
EED 6.15e-03
JUNB 6.68e-03
ESR1 1.03e-02
−log10(p-value)
F
Top 10 Reactome Canonical Pathways
Extracellular Matrix Organization
Cytoprotection by HMOX1
RHO GTPases Activate ROCKs
Muscle Contraction
Turbulent Flow Shear Stress Activates Signaling by PIEZO1 and Integrins in Endothelial Cells
Non-integrin membrane-ECM Interactions
RHO GTPase Cycle
Signaling by Rho GTPases
Signaling by Rho GTPases, Miro GTPases and RHOBTB3
ECM Proteoglycans
-log 10 (p-value)
Transcription Factor PPIs
SMAD2 *8.64e-08
SMAD3 *5.40e-06
SP1 *6.12e-06
NR3C1 *1.05e-05
NOTCH1 *1.05e-05
ESR1 *1.38e-05
BCL3 *2.21e-05
CLOCK *2.28e-05
SMAD1 *3.13e-05
KLF5 *7.01e-05
−log10(p-value)

FIGURE 3

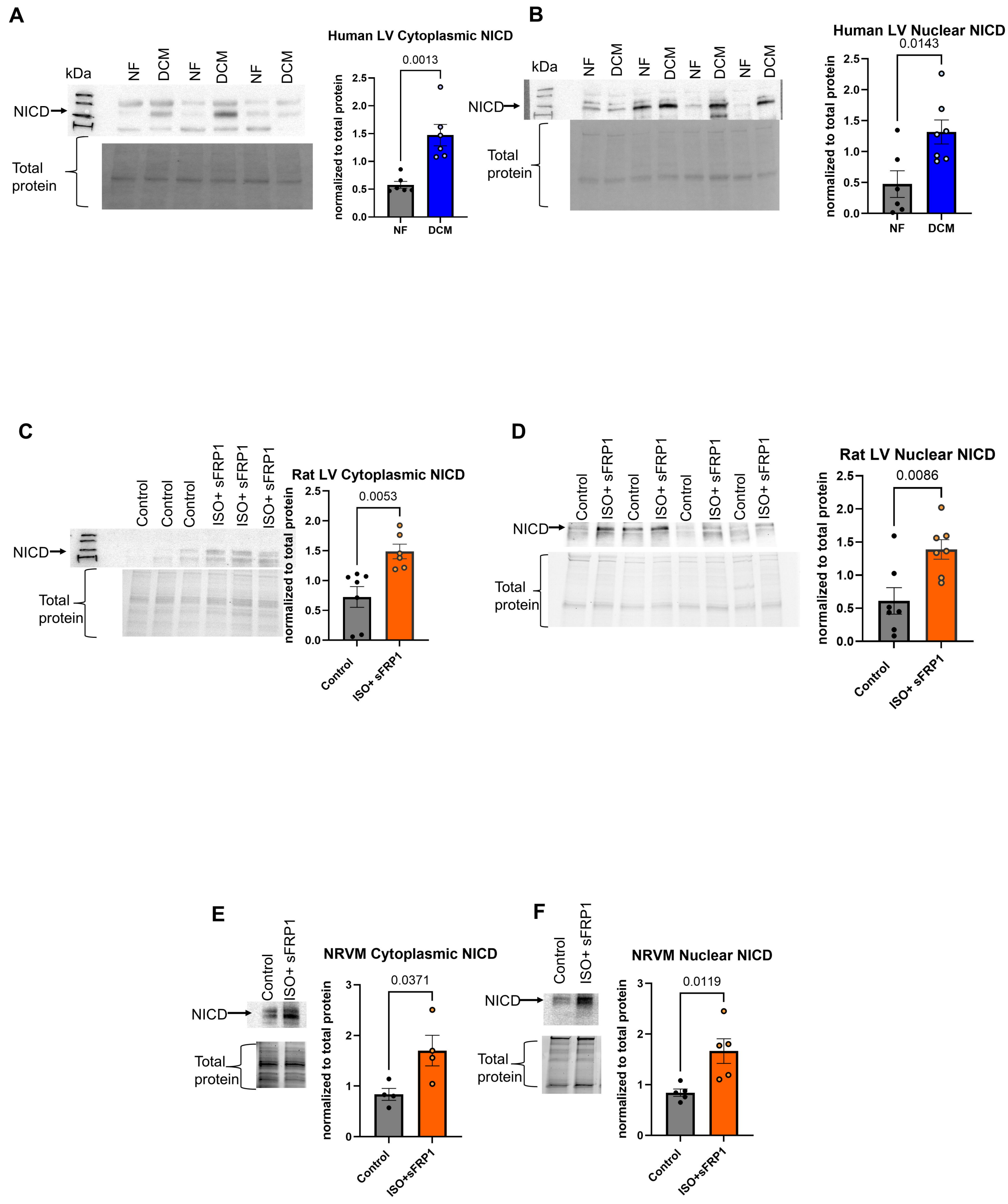
A
kDa
NF
DCM
NF
DCM
NF
DCM
NICD
Total protein
Human LV Cytoplasmic NICD
0.0013
normalized to total protein
2.5
2.0
1.5
1.0
0.5
0.0
NF
DCM
B
kDa
NF
DCM
NF
DCM
NF
DCM
NICD
Total protein
Human LV Nuclear NICD
0.0143
normalized to total protein
2.5
2.0
1.5
1.0
0.5
0.0
NF
DCM
C
Control
Control
Control
ISO+ sFRP1
ISO+ sFRP1
ISO+ sFRP1
NICD
Total protein
Rat LV Cytoplasmic NICD
0.0053
normalized to total protein
2.5
2.0
1.5
1.0
0.5
0.0
Control
ISO+ sFRP1
D
Control
ISO+ sFRP1
Control
ISO+ sFRP1
Control
ISO+ sFRP1
Control
ISO+ sFRP1
NICD
Total protein
Rat LV Nuclear NICD
0.0086
normalized to total protein
2.5
2.0
1.5
1.0
0.5
0.0
Control
ISO+ sFRP1
E
Control
ISO+ sFRP1
NICD
Total protein
NRVM Cytoplasmic NICD
0.0371
normalized to total protein
3
2
1
0
Control
ISO+sFRP1
F
Control
ISO+ sFRP1
NICD
Total protein
NRVM Nuclear NICD
0.0119
normalized to total protein
3
2
1
0
Control
ISO+sFRP1

FIGURE 4

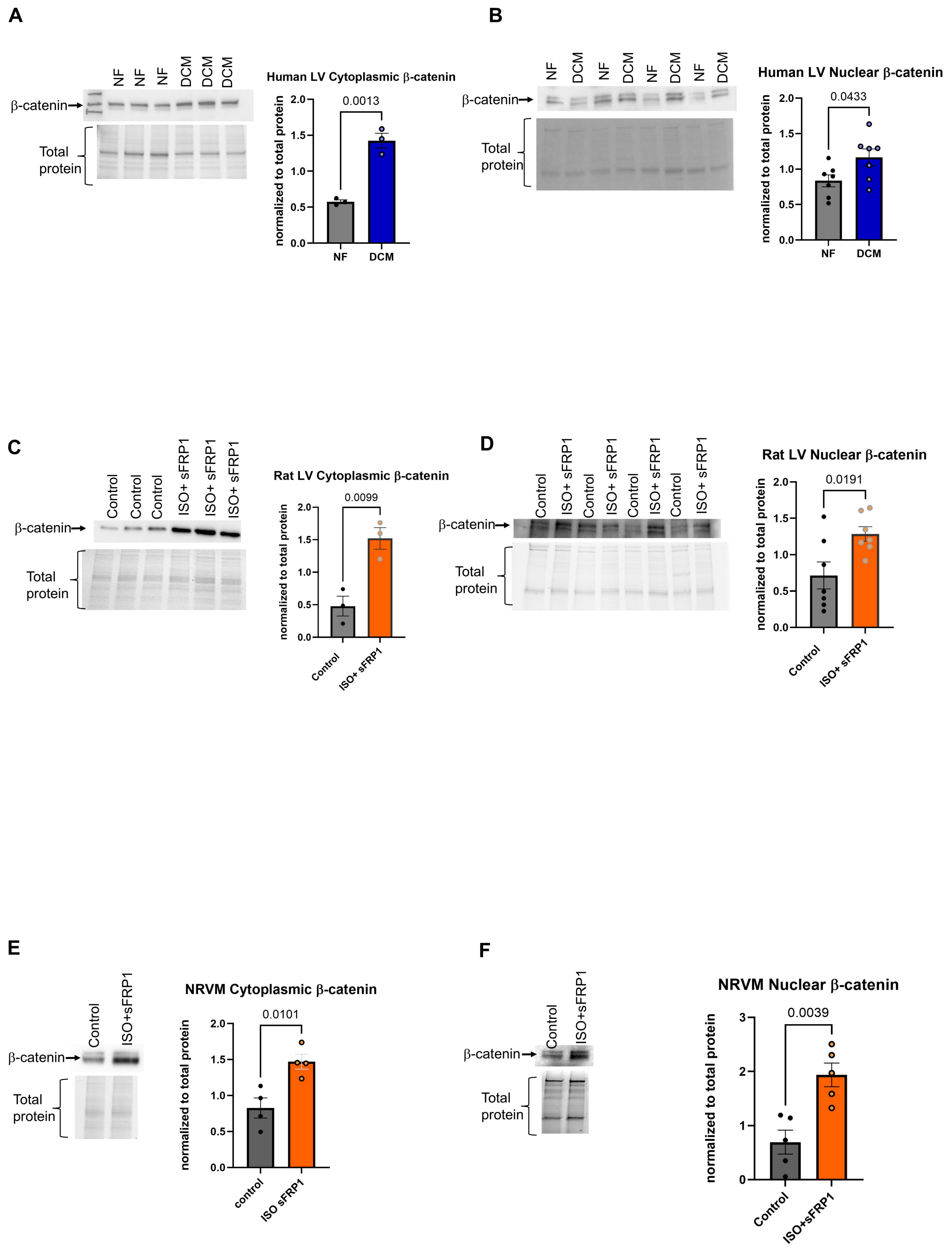
A
NF
NF
NF
DCM
DCM
DCM
β-catenin
Total protein
Human LV Cytoplasmic β-catenin
0.0013
normalized to total protein
2.0
1.5
1.0
0.5
0.0
NF
DCM
B
NF
DCM
NF
DCM
NF
DCM
β-catenin
Total protein
Human LV Nuclear β-catenin
0.0433
normalized to total protein
2.0
1.5
1.0
0.5
0.0
NF
DCM
C
Control
Control
Control
ISO+ sFRP1
ISO+ sFRP1
ISO+ sFRP1
β-catenin
Total protein
Rat LV Cytoplasmic β-catenin
0.0099
normalized to total protein
2.0
1.5
1.0
0.5
0.0
Control
ISO+ sFRP1
D
Control
ISO+ sFRP1
Control
ISO+ sFRP1
Control
ISO+ sFRP1
Control
ISO+ sFRP1
β-catenin
Total protein
Rat LV Nuclear β-catenin
0.0191
normalized to total protein
2.0
1.5
1.0
0.5
0.0
Control
ISO+ sFRP1
E
Control
ISO+sFRP1
β-catenin
Total protein
NRVM Cytoplasmic β-catenin
0.0101
normalized to total protein
2.0
1.5
1.0
0.5
0.0
control
ISO sFRP1
F
Control
ISO+sFRP1
β-catenin
Total protein
NRVM Nuclear β-catenin
0.0039
normalized to total protein
3
2
1
0
Control
ISO+sFRP1

FIGURE 5

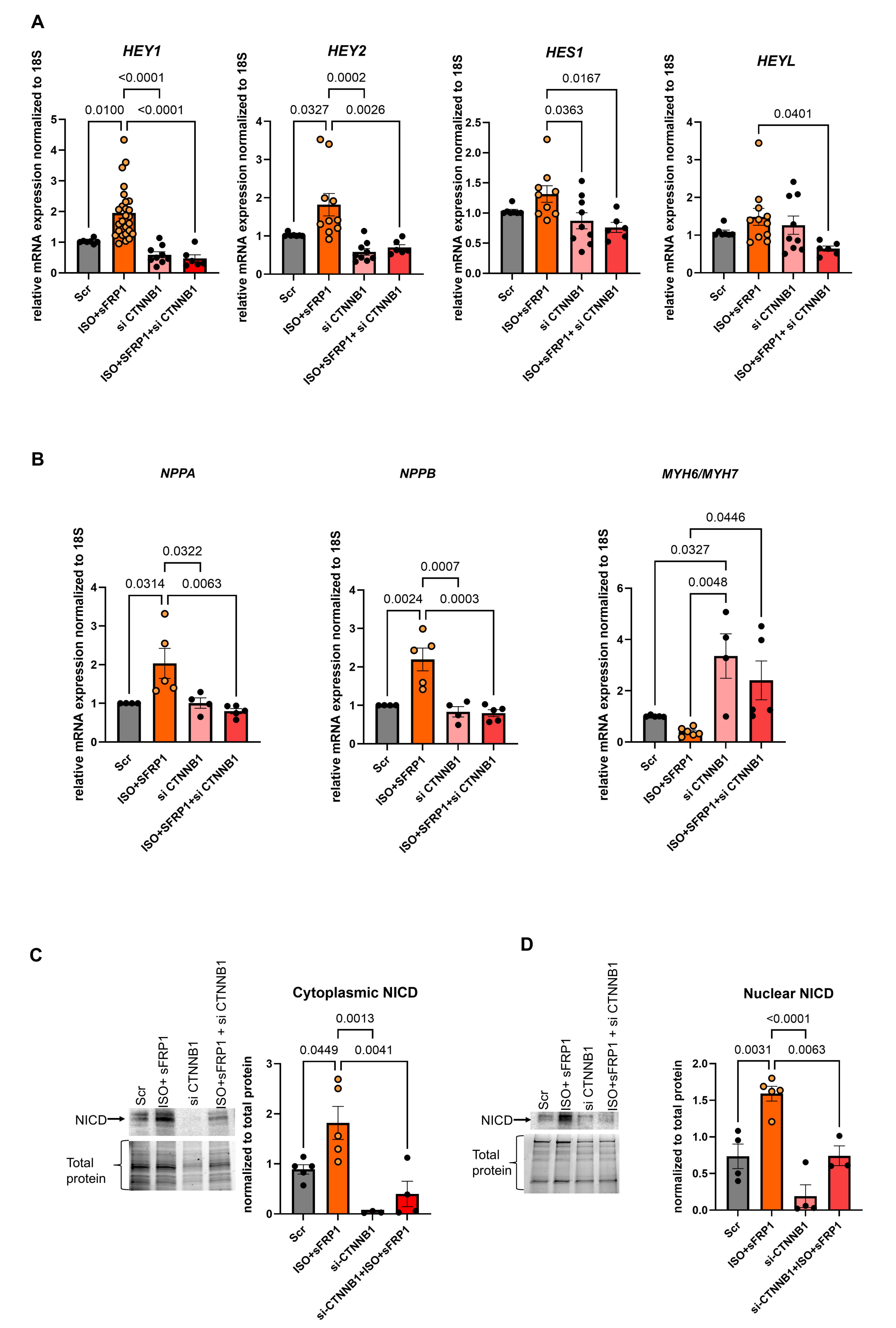
A
HEY1
HEY2
HES1
HEYL
relative mRNA expression normalized to 18S
<0.0001
0.0100
<0.0001
0.0002
0.0327
0.0026
0.0167
0.0363
0.0401
Scr
ISO+sFRP1
si CTNNB1
ISO+SFRP1+si CTNNB1
B
NPPA
NPPB
MYH6/MYH7
0.0322
0.0314
0.0063
0.0007
0.0024
0.0003
0.0446
0.0327
0.0048
C
Cytoplasmic NICD
0.0013
0.0449
0.0041
normalized to total protein
NICD
Total protein
Scr
ISO+ sFRP1
si CTNNB1
ISO+sFRP1 + si CTNNB1
ISO+sFRP1
si-CTNNB1
si-CTNNB1+ISO+sFRP1
D
Nuclear NICD
<0.0001
0.0031
0.0063
si-CTNNB1+ISO+sFRP1

FIGURE 6

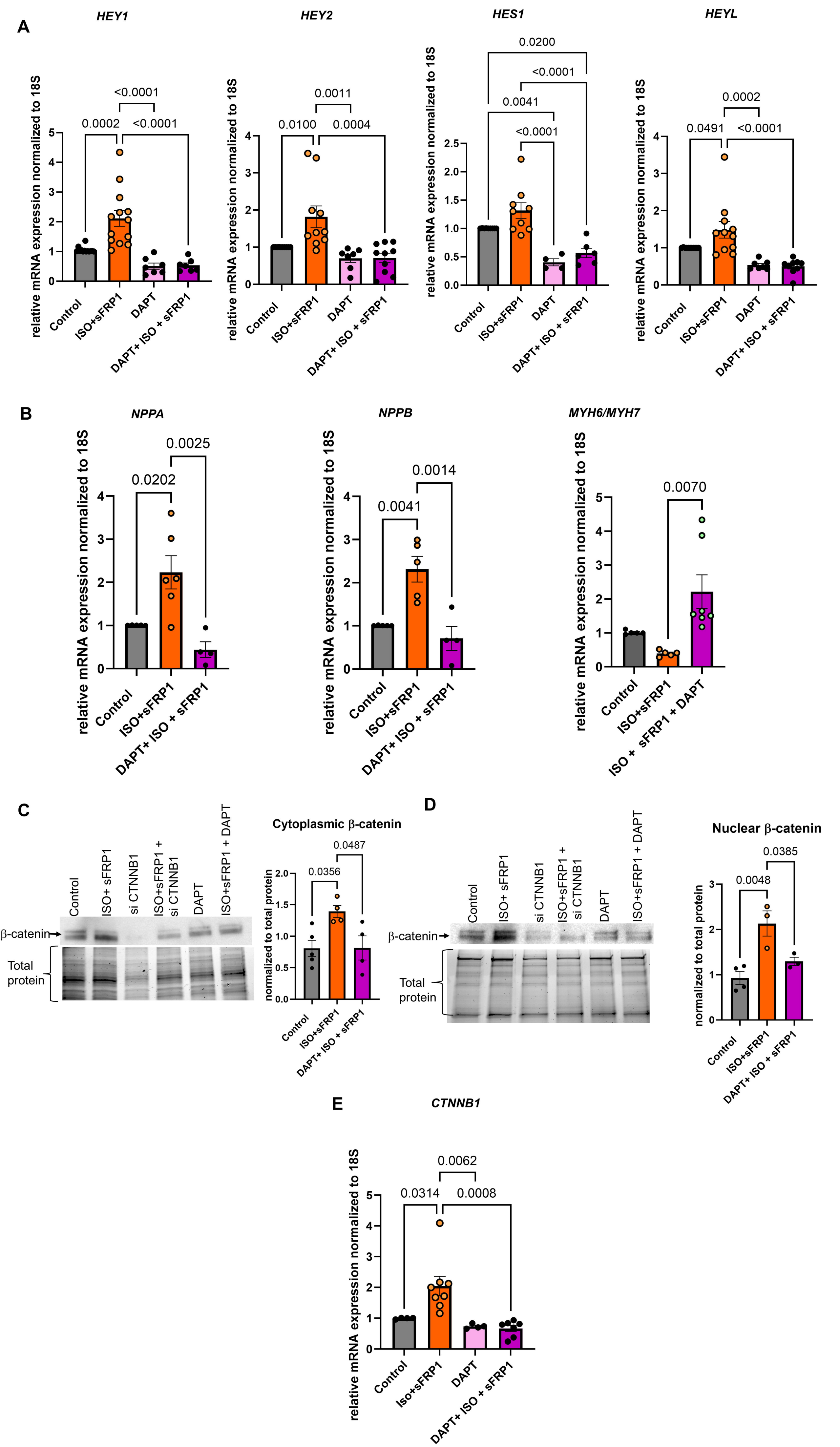
A
HEY1
HEY2
HES1
HEYL
relative mRNA expression normalized to 18S
<0.0001
0.0002
<0.0001
0.0011
0.0100
0.0004
0.0200
<0.0001
0.0041
<0.0001
0.0002
0.0491
<0.0001
Control
ISO+sFRP1
DAPT
DAPT+ ISO + sFRP1
B
NPPA
NPPB
MYH6/MYH7
0.0025
0.0202
0.0014
0.0041
0.0070
ISO + sFRP1 + DAPT
C
Control
ISO+ sFRP1
si CTNNB1
ISO+sFRP1 + si CTNNB1
DAPT
ISO+sFRP1 + DAPT
β-catenin
Total protein
Cytoplasmic β-catenin
normalized to total protein
0.0487
0.0356
D
Nuclear β-catenin
0.0385
0.0048
E
CTNNB1
0.0062
0.0314
0.0008
Iso+sFRP1

FIGURE 7

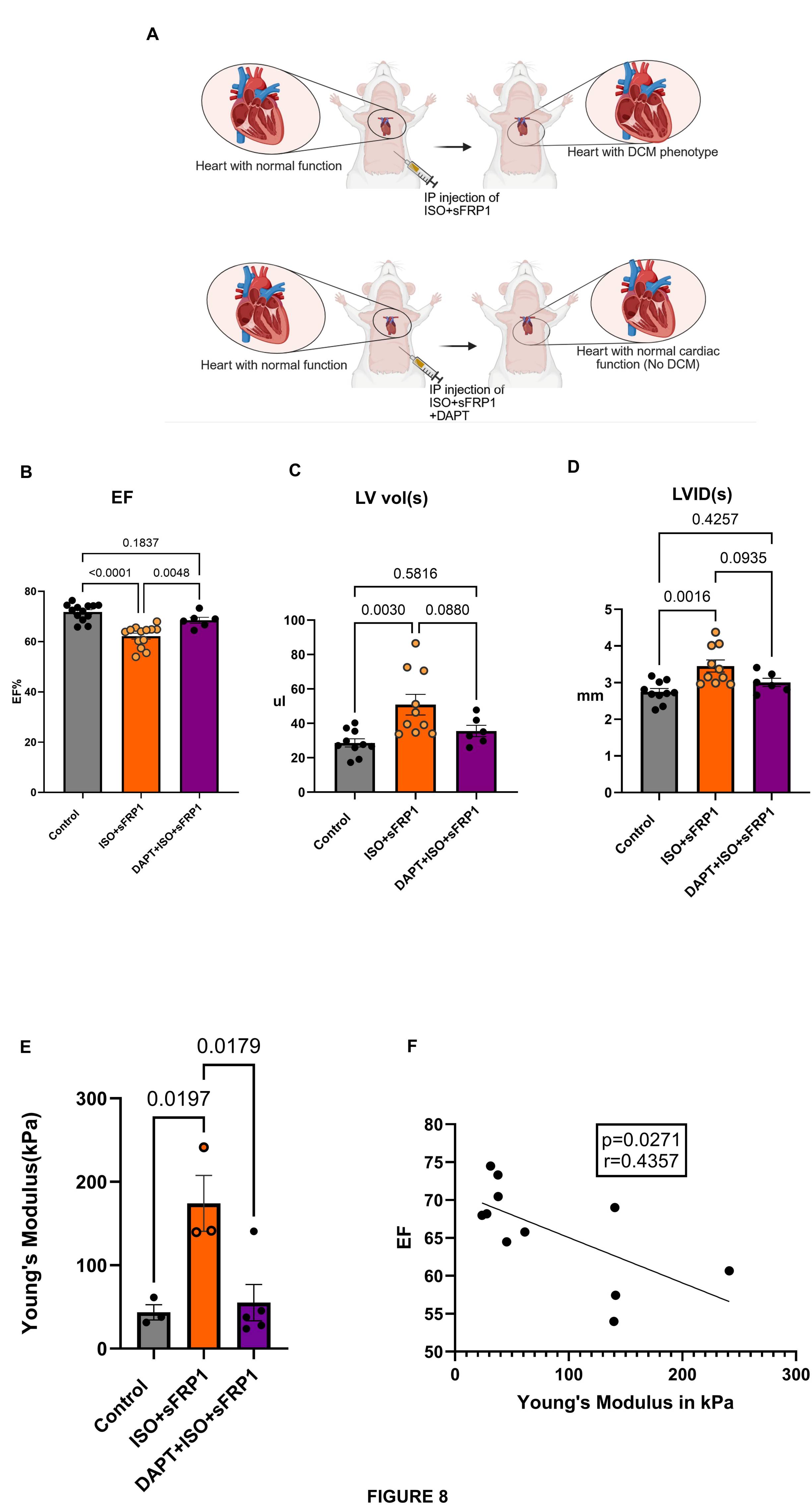
A
Heart with normal function
IP injection of ISO+sFRP1
Heart with DCM phenotype
Heart with normal function
IP injection of ISO+sFRP1 +DAPT
Heart with normal cardiac function (No DCM)
B
EF
0.1837
<0.0001
0.0048
EF%
Control
ISO+sFRP1
DAPT+ISO+sFRP1
C
LV vol(s)
0.5816
0.0030
0.0880
ul
Control
ISO+sFRP1
DAPT+ISO+sFRP1
D
LVID(s)
0.4257
0.0935
0.0016
mm
Control
ISO+sFRP1
DAPT+ISO+sFRP1
E
0.0179
0.0197
Young's Modulus(kPa)
Control
ISO+sFRP1
DAPT+ISO+sFRP1
F
p=0.0271
r=0.4357
EF
Young's Modulus in kPa

FIGURE 8